# WIND TUNNEL RESEARCH OF FLOWFIELDS WITHIN NATURALLY VENTILATED ROOMS OF SIMPLE GEOMETRY

by

M. Poreh,[1] J. E. Cermak,[2] and J. A. Peterka[3]

prepared for

Florida Solar Energy Center
300 State Road 401
Cape Canaveral, Florida 32920

Under

DOE Contract No. DE-AC03-80CS11510

Fluid Mechanics and Wind Engineering Program
Fluid Dynamics and Diffusion Laboratory
Colorado State University
Fort Collins, Colorado 80523

September 1982

CER82-83MP-JEC-JAP17
Project Number: 5-35663

[1]Visiting Professor, CSU, Professor of Environmental and Water Resources Engineering, Technion/Israel Institute of Technology

[2]Professor-in-Charge, Fluid Mechanics and Wind Engineering Program, and Director, Fluid Dynamics and Diffusion Laboratory, CSU

[3]Associate Professor of Civil Engineering, CSU

## TABLE OF CONTENTS

## LIST OF TABLES

## LIST OF FIGURES

## LIST OF SYMBOLS

| Symbol | Definition | Units |
|---|---|---|
| a | Configuration A, as shown in Statement of Work | (-) |
| A | Area of aperture | ($m^2$) |
| b | Configuration B, as shown in Statement of Work | (-) |
| B | Building | (-) |
| c | Configuration C, as shown in Statement of Work | (-) |
| $C_F$ | $1 + (A_{inlet}/A_{outlet})^2$ | (-) |
| $C_p$ | Coefficient of pressure $\frac{P}{\rho\, V_p^2/2}$ | (-) |
| $C_{p_s}$ | Static pressure coefficient | (-) |
| $C_{p_t}$ | Total pressure coefficient | (-) |
| $H_B$ | External height (10.35) of building model | (cm) |
| $H_I$ | Internal height (9.75) of model | (cm) |
| $H_p$ | Height (137.8) of pitot-static tube | (cm) |
| $H_w$ | Mid-height (4.88) of windows | (cm) |
| L | Interior length/width (29.26) of model | (cm) |
| p | Pressure | ($N/m^2$) |
| P | Dynamic pressure | ($N/m^2$) |
| Re | Reynolds number $\frac{V_w}{V_p} \left(\frac{V_p H_I}{\nu}\right)$ | (-) |
| $\bar{\mu}$ | Mean velocity | (m/s) |
| $V_1$ | Velocity measured near upwind plane of aperture | (m/s) |
| $V_2$ | Velocity measured near downwind plane of aperture | (m/s) |
| $V_{aW}$ | Mean velocity in flow measured at center of Configuration A Inlet | (m/s) |
| $V_{bW}$ | Mean velocity in flow measured at center of Configuration B Inlet | (m/s) |

| Symbol | Definition | Units |
|---|---|---|
| $V_B$ | Mean velocity in approach flow at 10.35 cm building height | (m/s) |
| $V_c$ | Velocity calculated to coincide with plane of total pressure measurements | (m/s) |
| $V_{cW}$ | Mean velocity in flow measured at center of Configuration C Inlet | (m/s) |
| $V_p$ | Reference velocity measured with pitot-static tube | (m/s) |
| $V_W$ | Mean velocity in approach flow at 4.88 cm height | (m/s) |
| X | Longitudinal coordinate | (cm) |
| Y | Lateral coordinate | (cm) |
| Z | Vertical coordinate | (cm) |

Greek Symbols

| | | |
|---|---|---|
| $\Delta$ | Net change in condition | (-) |
| $\rho$ | Density of air | $(Kg/m^3)$ |
| $\sigma$ | Standard deviation | (-) |
| $\nu$ | Kinematic viscosity of air | $(m^2/s)$ |

Subscripts

| | | |
|---|---|---|
| m | Model | (-) |
| rms | Root-mean-square of quantity | (-) |

## INTRODUCTION

A major factor in determining the efficiency of cooling and of increasing the comfort of people by natural ventilation is the distribution of the mean velocity and the turbulence intensity inside the ventilated building. These distributions are determined by the interior shape of the building and the conditions at the inlet and outlet apertures, which in turn depend on the exterior building shape and wind field.

A cooperative research program devoted to studies of natural ventilation was established between the Florida Solar Energy Center (FSEC) and the Fluid Mechanics and Wind Engineering Program at Colorado State University (CSU).* The study described in this report consisted of wind-tunnel experiments to determine the flowfield created within a box-like structure containing two windows. Three configurations of the structure were investigated in the Meteorological Wind Tunnel of the Fluid Dynamics and Diffusion Laboratory at CSU. The pressure distributions on the closed windows and the pressure at the same locations with open windows were measured and related to the approach flow. The mean air speed and the turbulence intensities near the windows and at various locations inside the rooms were measured using an omnidirectional hot-film probe and a vertical, cylindrical hot-film probe. The air speed inside the room and at the windows was related to the approach flow and the pressures on the closed windows. Flow visualization using smoke and cotton tufts was used to study the flow patterns and the direction of the air flow at various locations inside each

*A previous wind-tunnel study on natural ventilation was reported by Cermak (October 1981).

structure. Black and white photographs showing the basic features of the flow are presented in the report. Color slides and motion pictures are provided as supplements to this report.

## EXPERIMENTAL CONFIGURATIONS, EQUIPMENT AND PROCEDURES

### Wind Tunnel

All experiments were conducted in the downstream end of the Meteorological Wind Tunnel (MWT) at the turntable location. Design and operation of the MWT are described in detail by Cermak (June 1981). Elevation and plan views of the tunnel are contained in Figure 1 to this report.

Similarity criteria for physical modeling of the atmospheric boundary layer (ABL) are presented by Cermak (1971). The relatively small (1:25) scale of the models combined with the two meter height limitation of the MWT created a problem in simulating the entire depth of the ABL (300 m to 500 m). Fortunately, the difficulty was eliminated by simulating only the atmospheric surface layer (ASL) which consists of the lower layer of the ABL (approximately 100 m) and is characterized by nearly constant shear stress. The reader is directed to Cook (1978) and Cermak (October, 1982) for comprehensive explanations of ASL simulations in wind-tunnel flows. Wooden spires, 1.83 m tall, a 0.18 m trip and 20 cm roughness cubes were located near the MWT entrance (see Figure 2) to develop the desired portion of the boundary layer. The remainder of the test section floor was covered with roughness cubes and smooth "Masonite", as illustrated in Figure 3.

Figure 4 schematically portrays the test locations. The hot-film probes were inserted through a hole in the floor of the wind tunnel, 114 cm downstream from the 1.25 cm roughness. The floorless model was positioned on the "Lucite" floor and tightly attached to it, using an adhesive tape, to prevent leakage and possible displacement. Its position for each measurement or flow visualization was determined by the relative position of the hot film or tufts for that experiment. In all the experiments the building face was normal to the mean ambient flow in the wind tunnel, see Figs. 5 and 6.

Since the flow in the central section of the wind tunnel is two-dimensional and since the longitudinal variation of the mean motion without the building is very mild, the effect of shifting the position of the model in the wind tunnel, by at most ±14 cm, is expected to be negligible.

## Model Construction

The 1:25 scale models of the one-room buildings were constructed from 5 mm transparent plastic ("Lucite"). Each model included the walls and roof of the building. The floor of the wind tunnel, on which the model rested, served as a floor for the structures, as shown in Figs. 4, 5 and 6.

A view of the model, its dimensions, the location and dimensions of windows, for the three configurations, are shown in Figs. 7 and 8. Note the sharp edges at the interior side of each window, as shown in Figs. 4 and 8.

## Pressure Measurements

The location and notation of the pressure ports for each configuration are shown in Fig. 9. Pressure taps were located as requested in the statement of work. Three additional taps were located on either side of the inlets/outlets utilizing the same relative spacing. The 1/16 inch I.D. pressure ports were connected by 1/16 inch I.D. plastic tubing to a rotary valve which in turn connected each port to a Setra Differential Transducer (Model 237) with a 0.1 psid range, see Fig. 6. The reference side of the transducer was connected to the static side of a pitot-static tube mounted high in the wind tunnel. The same tube was also used to simultaneously measure the mean velocity at that height, which was adjusted for each run to $V_p = 10$ m/sec. The output from the transducer was routed through a differential amplifier to an "on-line" data acquisition system.

The FDDL on-line data system consists of a Preston Scientific analog-to-digital convertor, a Hewlett-Packard 21 MX computer, disk unit, card reader, printer, and a Digi-Data digital tape drive. The filtered and converted transducer signals are immediately processed into pressure coefficient form and stored for printout or further analysis.

The pressure at each port was measured for 16 seconds at a rate of 250 samples per second. Extensive experience indicates that the overall accuracy of the pressure measurements (in dimensionless pressure coefficient form based on $0.5\ \rho V_p^2$) is 0.03 for mean pressures, 0.1 for peak pressures, and 0.01 for rms pressures.

A rake of nine total pressure tubes (see Figure 10) placed inside the model was used to measure the pressure in the downstream plane of each inlet window. The pressure tubes were positioned perpendicular to the plane of the window and at the same vertical and lateral locations used for the closed window pressure ports. The rakes were also placed outside the model, in the downstream plane of the outlet windows, for measuring the pressures at those windows. The same notation was used to identify the rake pressure tubes as was used to identify the pressure ports, see Fig. 9.

## Mean Speed and Turbulence Intensity Measurements

An omni-directional spherical hot-film probe on a vertical stem, was used to measure the mean airspeed. The probe, shown in Fig. 11, was manufactured by TSI Inc. (TSI-Model 1620). Calibration of the probe in the wind tunnel revealed that directional sensitivity of the probe to winds with relatively small vertical components, up to ±30° from the vertical axis was ±3%. The response of the probe is too slow to be used for measuring turbulence.

A fast response vertical cylindrical hot-film probe (TSI-1211-10), see Fig. 11, was also used in the study. It was found, however, that this probe, which can measure only the horizontal velocities, had rather high directional sensitivity due to the effect of the supporting prongs. It was thus used only to measure the turbulence inside the room as well as in the approach flow, where its orientation, relative to the flow, was the same as in the calibration.

All the velocity measurements were taken at $V_p$ = 10 m/sec. Tunnel speed was set at the start of each workday and closely monitored throughout the conduct of all experiments. Tolerance was maintained within ±1.0% at the 10 m/s freestream speed selected for the research experiments. Tunnel speed was maintained during most model reconfigurations to eliminate the need for re-establishing the selected reference velocity. This procedure also minimized the introduction of changes to the reference velocity.

## Flow Visualization

Two techniques were used for flow visualization. In one experiment cotton swabs saturated with titanium tetrachloride were placed at various points inside and adjacent to the model. The titanium tetrachloride smoke was illuminated with arc-lamps after covering the acrylic base with nonreflecting paper to reduce the glare. Photography was accomplished with a 16 mm Bolex movie camera and a Canon F-1 35 mm camera loaded with black and white ASA-400 film and set to f5.6 stop and 1/60th-second shutter speed. The wind tunnel speed during the visualizations with the smoke was reduced to approximately $V_p$ = 2 m/sec.

A second visualization study utilized white cotton tufts, glued to small pins which were inserted in 1/32 I.D. brass tubes, as shown in Figure 12. The tubes were affixed to the floor of the tunnel at necessary intervals. Usually seven tufts were placed at the same lateral distance, Y/L, from the wall and were photographed simultaneously. The lateral position Y/L was changed by sliding the model sideways. The response time of the tufts to changes in the direction of the turbulent flow was relatively short and they continuously changed their orientation according to the "instantaneous" large scale motion at their location.

The camera was positioned 1.5 m above the model and three one-second exposures of the tufts were taken at each position with the Canon F-1 35 mm camera loaded with EPT 160 color slide film. Additional tuft photographs were produced from black and white enlarged prints of the color slides. The photographs of the tufts placed at mid-height of the room (Z/H = 0.5) were also combined into mosaics to provide an overall view of the flow pattern for each configuration. The wind tunnel speed during these experiments was set at approximately $V_p$ = 10 m/sec.

## PRESENTATION AND ANALYSIS OF THE EXPERIMENTAL RESULTS

### Flow Visualization

Typical one-second exposures of a row of 7 cotton tufts, located in this case at Z/H = 0.5, Y/L = 0.95, and X/L = 0.1, 0.25, 0.33, 0.50, 0.66, 0.75 and 0.9 in Configuration B, are shown in Fig. 13. The X, Y, Z coordinate system is defined in Fig. 7. Only slight differences between the two one-second exposures can be observed. However, considerable differences are observed in the two exposures at Y/L = 0.9, in Configuration A, shown in Fig. 14. Observation of the tufts at these locations has also indicated that the mean direction of the flow in some positions is not clearly defined. Certain tufts orient themselves in a given direction for a short time, move slightly around that direction and suddenly change their orientation drastically, as evident from Fig. 14, for example.

The lack of a well-defined mean orientation at many points made it initially difficult to explain the recorded results. However, when the number of the tufts was increased and their photographs at the various locations were combined, a clear picture of the flow structure in each configuration emerged.

Figure 15 shows one side of the symmetrical internal flow in Configuration B (this configuration is presented first because of the clear structure of its internal flow.) One sees in the picture that all the tufts at the axis of symmetry Y/L = 0.5 are oriented along that axis toward the outlet window. The motion of the tufts suggests an increasing intensity of the large scale turbulence in the direction of the flow, as found in air jets. The figure also indicates that the flow in the central region, between the small inlet window and the larger outlet window, is producing an enlongated vortex motion at each side. The tuft located at X/L = 0.5 and Y/L = 0.75 is located near the center of this vortex and is continuously changing its direction.

Figure 16 shows photographs of the smoke visualization for Configuration B. Figure 16a was taken after filling the entire room with smoke. The jet of clean air entering the room is clearly observed in this photograph. One also sees that the size of the eddies created by the jet flow is close to that of the width of the inlet window. It is also evident from the pattern of the smoke that the flow is very turbulent and that the large scale vortex motion at the sides of the room is constantly perturbed by the turbulent eddies.

The structure of the flow in Configuration A, where the inlet window is wider than the outlet window, is more complex as can be seen in Figs. 17 and 18. The tufts close to the inlet window show that the air flow there is more turbulent than in Configuration B. A vortex motion is observed in these figures, however, the larger eddies often break this motion and distort it and the overall character of the flow in the room is highly time dependent. Close to the small outlet window the flow accelerates and the size of the turbulent eddies is reduced, as evident by the attenuated lateral motion of the tuft near that window.

The flow in Configuration C, see Figs. 19 and 20 is the most complex because of its assymmetrical shape. Figure 19 shows that the initial direction of the jet entering the room is approximately normal to that window. However, it rapidly changes its direction toward the outlet window, as clearly seen in Fig. 20. On the opposite side of the room, a clear large vortex is created, as seen in these photographs.

The motion at the lower left-hand corner appears to be a part of this vortex. On the other hand, the direction of the flow in the upper left corner between the two windows, is not very clear. It is interesting to note that the direction of the flow leaving the outlet window is initially almost normal to the plane of the window. A short distance downstream, however, it sharply curves in the direction of the ambient flow.

Additional photographs of tufts in the windows and at different heights, provided in supplements, show that the flow is almost normal to the plane of the window. However, one can see the contraction of the air jet as it enters the room, from the position of the side tufts.

## Velocity and Turbulence Measurements in the Approach Flow

Figure 21 shows the mean velocity and turbulence intensity distribution profiles in the approach flow above the 1.25 cm roughness, 114 cm upstream from the mean location of the model (see Fig. 4). The profiles were obtained with a TSI Model 1211-10 hot-film sensor. Voltage output was sampled 100 times per second for 30-60 seconds at each of the indicated heights. Table 1 contains specific values for each of the subject profiles. The freestream velocity, $V_p$, measured with a pitot-static tube located as shown in Figure 4, was used to monitor tunnel speed during all experimental velocity measurements. Pressure was monitored with a MKS Baratron pressure meter and averaged over several minute intervals with an H-P integrating digital voltmeter to insure the accuracy of speed settings.

The ratio of the mean velocity in the approach flow at the height of the center of the window $H_W = 4.88$ cm, to $V_p$, was

$$\frac{V_W(4.88\ \mathrm{cm})}{V_p} = 0.49\ .$$

At the height of the building $H_B$ = 10.35 cm the value of this ratio was

$$\frac{V_B(10.35\ \mathrm{cm})}{V_p} = 0.58\ .$$

The absence of roughness in the neighborhood of the model is expected to cause an immediate acceleration of the flow at that region. Indeed, when the model was removed the velocity ratio at its mean location was

$$\frac{V_m(4.88\ \mathrm{cm})}{V_p} = 0.59\ .$$

The longitudinal variation in the neighborhood of the house makes it impossible to choose a unique representative velocity for the approach flow. On the other hand, this variation is typical of many prototype conditions where the roughness in the immediate neighborhood of a house is small compared to the average roughness of the upstream area, which is determined by both the roughness of the terrain and the drag on the buildings and trees.

Pressure Measurements

The measurements of the pressure on the envelope of the closed building, at the locations of the windows, for the three configurations are presented in dimensionless form in Tables 2a, 2b, and 2c.

The dimensionless pressure coefficient is the ratio of the measured pressure, above the ambient pressure in the tunnel, to the dynamic pressure of the pitot-static tube:

$$C_p = \frac{P}{\rho V_p^{\ 2}/2}\ .$$

Since the pressure ports on the front walls of Configurations A and C are located in identical positions, the data for the two models have been compared in order to evaluate the accuracy of the measurements. The average pressure coefficients on the two front windows, calculated by averaging the pressure coefficients measured at the pressure ports 2, 3, 4, 7, 8, 9, 12, 13 and 14, were $C_p = 0.210$ and $C_p = 0.206$, namely

$$C_p = 0.208 \pm 1\% \ .$$

The standard deviation of the differences between the individual pressure coefficients at these ports was

$$\sigma = 0.014 \ (7\%) \ .$$

The average pressure coefficient on the small front window in Configuration B is also very close to the above values

$$C_p = 0.212 \ .$$

These coefficients appear to be small numbers. One should recall, however, that the reference pressure was taken as the dynamic pressure at the upper edge of the boundary layer. If one uses for reference the dynamic pressure of the approach velocity at mid-height of the window, the pressure coefficients are increased by a factor of 4,

$$\tilde{C}_p = C_p \cdot \left(\frac{V_p}{V_W}\right)^2 = \frac{0.208}{(0.49)^2} = 0.86 \ .$$

As seen from the recorded data, the pressure coefficients on the outlet windows were slightly negative:

$$C_p(A) = -0.091; \ C_p(B) = -0.096; \text{ and } C_p(C) = -0.106 \ .$$

It is noted that the pressure distribution on the windows is not uniform. The horizontal variations in Configurations A and B are small, but large differences are observed between the ports 2, 3, and 4 at z = 6.5 cm and the ports 12, 13, and 14 at z = 3.25 cm. The average values recorded at these ports in configuration A, for example, were $C_p = 0.24$ at the upper row and $C_p = 0.18$ at the lower row.

The vertical distribution of the pressure on the outlet windows in Configurations A and B was much more uniform $\bar{C}_p = -0.095$ and $\bar{C}_p = -0.083$, in Configuration A, for example. On the other hand, considerable horizontal nonuniformity is observed on the area of the outlet window of Configuration C, which is parallel to the mean ambient flow. The pressure ports 2, 7 and 12, at this window, have recorded a pressure coefficient $C_p = -0.144 \pm 0.005$, whereas the pressure coefficient at the downwind ports 4, 9 and 14 was $C_p = -0.076 \pm 0.005$.

The values of the total pressure coefficients at the open windows, measured at the exit plane of each window (see Fig. 22) are shown in the first column of Tables 3a, 3b and 3c. It is obvserved that the total pressures at the open inlet windows are slightly larger than the pressures measured on the outer enevelope of the closed models at the same points. This is not the case, however, for the outlet windows. The average total pressure coefficient downwind from the outlet windows in Configurations A and C were positive, whereas the total pressure at the outlet window of Configuration B was slightly negative (-0.011). The inlet window in Configuration B, it should be recalled, has a relatively small area. Thus, most of the combined pressure drop across the inlet and the outlet windows is expected to occur at the inlet window. Since the velocities at the large outlet window are also small, the total pressure at that window are also expected to be small, slightly above the ambient pressure at the back wall (-0.096). It will be seen later that the dimensionless dynamic head of the average exit velocity at that window was $(V/V_p)^2 = 0.065$ (Table 4b).

Velocities at the Windows

The shape of the velocity probes made it impossible to measure the mean velocities at the exact position of the total pressure measurements. The mean velocities were therefore measured at two planes: $V_1$, upstream of the window, and $V_2$, downstream from the window, as shown in Fig. 22. In all instances, voltage output of the probes was sampled for a thirty-second interval at a rate of one-hundred Hertz and relayed to the on line computer system via an analog-to-digital convertor. The average values of velocity and turbulence provided by the computer were used to calculate the dimensionless ratios of $V_1/V_p$ and $V_2/V_p$ which are given in Tables 4a, 4b and 4c. The mean velocities at the inner planes were also measured with the vertical hot-film which also recorded the local turbulent intensities, there.

The tables reveal that the velocities at the downwind side of each window were always larger than those at the upwind side, particularly for the small square windows (the outlet window in Configuration A and the inlet window in Configuration B) where the ratio of the two velocities was approximately 0.7. This difference is, of course, due to the contraction of the jet-type flow. These ratios for the large rectangular windows of the three configurations varied between 0.76 to 0.9. The contraction in windows with a 2:1 aspect ratio is expected to be smaller, giving velocity ratios closer to one, but apparently it is also influenced by other flow parameters.

A longitudinal velocity profile along the axis passing through the centers of the inlet and outlet windows in Configuration B was also measured and is presented in Fig. 23. One sees, from the figure, an initial deceleration of the flow, as it approaches the house, and a subsequent acceleration toward the inlet window, and later in the room, due to the contraction.

A considerable reduction in the velocities is observed further downstream where the jet-like flow is expanding. Finally, one sees the acceleration of the flow toward the outlet window.

From the values $V_1$ and $V_2$, the velocity ratio is calculated at the plane of the total pressure measurements, using a linear interpolation. The calculated values $V_{cal}$ also appear in Tables 3a, 3b and 3c.

The "static" pressure coefficients $C_{p_s}$ at this plane were estimated from the equation

$$C_{p_s} = C_{p_t} - (V/V_p)^2_{calculated} \; .$$

The values of $C_{p_s}$ are also presented in the same tables.

The velocities at the inlet windows, which are usually the largest in the room can be estimated using the difference between the average static pressures $\Delta C_p$ on the envelope of the closed house. Assuming that the head losses in the system are equal to the sum of the velocity heads at the two windows one may write that

$$\Delta C_p = (V_{inlet}/V_p)^2 + (V_{outlet}/V_p)^2$$

or

$$\Delta C_p = \left(\frac{V_{inlet}}{V_p}\right)^2 C_F$$

where,

$$C_F = 1 + (A_{inlet}/A_{outlet})^2 \; .$$

Thus, one finds that

$$\frac{V_{inlet}}{V_p} = \left(\frac{\Delta C_p}{C_F}\right)^{\frac{1}{2}} \; .$$

The calculated values of the ratios

$$\frac{(V/V_p)}{(\Delta C_p/C_F)^{\frac{1}{2}}} ,$$

where $V/V_p$ are the measured velocity ratios at the downstream side of each window, are shown in Figs. 24a, 24b, and 24c. The average values of this coefficient for the inlet windows of the three configurations are 1.05, 1.00 and 0.93 indicating a good agreement with the simplified model. The values at the outlet window are also in agreement with the theory as their values should be larger by the factor $A_{inlet}/A_{outlet}$.

## Reynolds Number Independence Tests

Internal to external velocity ratios were measured with the omni-directional hot film probe at two locations (1 and 3, as described in Table 5) inside the room for each configuration, varying the external wind-tunnel speed.

Reynolds number independence tests were initially conducted on Configuration A internal locations 1 and 3 and Configuration C location 1, only. Later tests were completed to document independence for these two locations on all three configurations within the velocity range where experiments were conducted.

Figure 24 shows the measured velocity ratios plotted versus the internal Reynolds number of the flow, $Re_I$, based on the average velocity at the inlet window for each configuration and the interior height of the room H.

As seen from this figure the velocity ratios become practically independent of the Reynolds number only when

$$Re_I > 2x10^4 .$$

The results are consistent with the criteria for Reynolds number independence proposed by Cermak (October 1982), which were based on an earlier natural ventilation wind-tunnel study.

Mean Velocities and Turbulence Intensities Inside the Rooms

The measured values of the mean velocity ratios $(V/V_p)$ and the turbulence intensities (TI) at various locations inside the rooms for the three configurations are presented in Tables 5a, 5b and 5c. Sampling procedures were as described for measurements in the window planes. The measurements at Z/H = 0.5 are also presented in Figs. 26a, 26b and 26c in dimensionless form, using two different reference velocities. The figures at the left show the distribution of the ratios

$$\frac{(V/V_p)}{(\Delta C_p/C_F)^{\frac{1}{2}}}$$

which describes the relative speed at each location using the theoretical average speed at the window $(\Delta C_p/C_F)^{\frac{1}{2}}$ as a reference. The above distribution is expected to depend primarily on the room-window configuration and probably would not change very much if the same room were a part of a larger building, as long as one uses the modified value of $(\Delta C_p/C_F)^{\frac{1}{2}}$ for the inlet window.

On the right side of the page the distribution of

$$\frac{V}{V_W}$$

is presented, where $V_W$ is the approach velocity at the same height (Z/H = 0.5). These ratios can be used to compare the combined efficiency of natural ventilation for different building and room configurations. For example, one sees from the figures that the inner mean velocities near the side walls for a given mean inlet velocity is larger in Configuration A than in Configuration B. However, as seen from the $V/V_W$ distributions, the actual mean velocities at this location for a given ambient speed would be larger in Configuration B, because the inlet mean speed for this configuration is larger than for Configuration A.

The local turbuence intensities in the three models appears to vary between 30% to 60%. Slightly larger values were measured in Configuration B.

## CONCLUSIONS

Mean velocity and turbulence measurements combined with flow visualization have been used to study the internal flow in a box-like one-room structure containing two windows. The study showed that the pattern of the flow inside the room is determined primarily by the jet of air entering the room from the inlet window. When the two windows are symmetrically located at the front and the rear of the room relative to the ambient velocity, two large vortices are created at the sides which are violently perturbed by turbulent eddies whose scale is of the same order as the window. When the second window is located at the side wall the jet flow inside the room orients itself toward that window creating a large vortex at the opposite side of the room.

The mean velocity distributions in the inlet windows are found to be non-uniform. The average value of the inlet velocity, however, can be closely estimated from the static pressure distribution on the envelope of the closed building. The mean velocities at mid-height inside the rooms are smaller than the velocity at the window, approximately 50 percent at the center of the room and 20-30 percent at the sides, depending on the location and the room-window configuration.

The turbulence intensities inside the rooms is usually very high, between 30 to 70 percent.

The overall character of the flow in the interior of the room is highly time independent with turbulent eddies with vertical axes forming from horizontal velocity gradients whose size is approximately that of the windows. These eddies were throughout the cavity causing fluctuations in the large standing eddies whose scale is of the order of half the room size.

## ACKNOWLEDGEMENTS

Planning for this study was accomplished through cooperation with Dr. Subrato Chandra of the Florida Solar Energy Center. His support of this study is appreciated by all the authors and technical support staff at Colorado State University.

The authors thank all technical support staff of the Fluid Dynamics and Diffusion Laboratory and Engineering Research Center who contributed to completion of this phase of the research program. In particular, the extensive assistance of Messrs. J. A. Beatty, J. C. Maxton, E. Spilman, C. Reynolds and C. Howell, is appreciated.

## REFERENCES

Cermak, J. E., "Laboratory Simulation of Atmospheric Boundary Layer," AIAA Journal, Vol. 9, No. 9, September 1971, pp. 1746-1754.

Cermak, J. E., "Wind Tunnel Design for Physical Modeling of Atmospheric Boundary Layer," Journal of the Engineering Mechanics Division, ASCE, Vol. 107, No. EM3, Proc. Paper 16340, June 1981, pp. 623-642.

Cermak, J. E., J. A. Peterka, S. S. Ayad, and M. Poreh, "Passive and Hybrid Cooling Developments: Natural Ventilation--A Wind-Tunnel Study, CER81-82JEC-JAP-SSA-MP24, October 1981.

Cermak, J. E. "Simulation of the Natural Wind," Preprint 82-518, ASCE Convention and Exhibit, New Orleans, Louisiana, 25-29 October 1982.

Cermak, J. E., M. Poreh, J. A. Peterka, and S. S. Ayad, "Wind-Tunnel Investigations of Natural Ventilation," Preprint 82-519, ASCE Convention and Exhibit, New Orleans, Louisiana, 25-29 October 1982.

Cook, N. J., "Determination of the Model Scale Factor in Wind Tunnel Simulations of Adiabatic Atmospheric Boundary Layer," Journal of Industrial Aerodynamics, Vol. 2, No. 4, 1978, pp. 321-331.

TABLES

Table 1. Mean Velocities and Turbulence Intensities Measured in the Approach Flow

| Data Point | Height (cm) | $\bar{u}$ (m/s) | $u_{rms}$ (m/s) | TI (%) |
|---|---|---|---|---|
| 1 | .50 | 2.47 | .727 | 29.36 |
| 2 | .68 | 2.54 | .712 | 28.02 |
| 3 | .97 | 2.79 | .788 | 28.26 |
| 4 | 1.24 | 3.08 | .862 | 27.99 |
| 5 | 1.55 | 3.42 | 1.352 | 39.52 |
| 6 | 1.95 | 3.82 | .987 | 25.80 |
| 7 | 2.44 | 4.03 | 1.023 | 25.39 |
| 8 | 2.95 | 4.36 | 1.026 | 23.55 |
| 9 | 3.47 | 4.31 | .981 | 22.74 |
| 10 | 4.00 | 4.64 | 1.065 | 22.97 |
| 11 | 5.04 | 4.88 | 1.038 | 21.25 |
| 12 | 7.07 | 5.41 | 1.014 | 18.75 |
| 13 | 9.98 | 5.68 | .969 | 17.05 |
| 14 | 13.04 | 6.08 | .997 | 16.40 |
| 15 | 16.02 | 6.32 | .947 | 14.98 |
| 16 | 20.02 | 6.54 | .962 | 14.71 |
| 17 | 25.06 | 6.91 | .960 | 13.88 |
| 18 | 30.05 | 7.06 | .905 | 12.83 |
| 19 | 40.01 | 7.73 | .901 | 11.66 |
| 20 | 50.01 | 8.15 | .860 | 10.56 |
| 21 | 60.04 | 8.47 | .826 | 9.74 |
| 22 | 75.00 | 9.22 | .716 | 7.76 |
| 23 | 90.00 | 9.73 | .620 | 6.37 |
| 24 | 105.06 | 10.09 | .528 | 5.23 |
| 25 | 119.92 | 10.19 | .489 | 4.80 |
| 26 | 125.96 | 10.21 | .433 | 4.24 |

Table 2a. Pressure Coefficients on the Closed Model of Configuration A

| Tap Number | Inlet | | Outlet | |
|---|---|---|---|---|
| | $\bar{C}_p$ | $C_{rms}$ | $\bar{C}_p$ | $C_{rms}$ |
| 1 | .241 | .104 | -.088 | .029 |
| 2 | .245 | .104 | -.095 | .030 |
| 3 | .226 | .095 | -.093 | .030 |
| 4 | .254 | .100 | -.097 | .029 |
| 5 | .256 | .099 | -.101 | .031 |
| 6 | .189 | .085 | -.091 | .030 |
| 7 | .211 | .091 | -.089 | .028 |
| 8 | .198 | .083 | -.095 | .028 |
| 9 | .218 | .087 | -.095 | .030 |
| 10 | .211 | .088 | -.104 | .032 |
| 11 | .170 | .077 | -.080 | .029 |
| 12 | .181 | .075 | -.085 | .031 |
| 13 | .171 | .072 | -.083 | .031 |
| 14 | .186 | .077 | -.087 | .030 |
| 15 | .189 | .080 | -.092 | .032 |
| Average (over window) | .210 | | -.091 | |

Table 2b. Pressure Coefficients on the Closed Model of Configuration B

| Probe Location | Inlet | | Outlet | |
|---|---|---|---|---|
| | $\bar{C}_p$ | $C_{rms}$ | $\bar{C}_p$ | $C_{rms}$ |
| 1 | .245 | .109 | -.098 | .031 |
| 2 | .234 | .093 | -.094 | .030 |
| 3 | .251 | .103 | -.097 | .029 |
| 4 | .241 | .099 | -.101 | .030 |
| 5 | .256 | .104 | -.106 | .033 |
| 6 | .209 | .090 | -.094 | .030 |
| 7 | .213 | .092 | -.090 | .030 |
| 8 | .211 | .088 | -.092 | .029 |
| 9 | .223 | .092 | -.099 | .028 |
| 10 | .207 | .091 | -.110 | .035 |
| 11 | .182 | .080 | -.093 | .033 |
| 12 | .170 | .070 | -.086 | .031 |
| 13 | .189 | .081 | -.088 | .031 |
| 14 | .179 | .073 | -.093 | .032 |
| 15 | .185 | .079 | -.100 | .035 |
| Average (over window) | .212 | | -.096 | |

Table 2c. Pressure Coefficients on the Closed Model of Configuration C

| Probe Location | Inlet | | Outlet | |
|---|---|---|---|---|
| | $\bar{C}_p$ | $C_{rms}$ | $\bar{C}_p$ | $C_{rms}$ |
| 1 | .238 | .100 | -.221 | .095 |
| 2 | .239 | .099 | -.142 | .087 |
| 3 | .244 | .106 | -.097 | .066 |
| 4 | .235 | .096 | -.077 | .058 |
| 5 | .239 | .101 | -.074 | .055 |
| 6 | .223 | .099 | -.213 | .099 |
| 7 | .191 | .083 | -.149 | .082 |
| 8 | .202 | .077 | -.102 | .060 |
| 9 | .204 | .088 | -.081 | .053 |
| 10 | .207 | .098 | -.068 | .049 |
| 11 | .171 | .077 | -.209 | .086 |
| 12 | .177 | .074 | -.140 | .076 |
| 13 | .185 | .080 | -.097 | .057 |
| 14 | .177 | .072 | -.071 | .053 |
| 15 | .177 | .080 | -.066 | .048 |
| Average (over window) | .206 | | -.106 | |

Table 3a. Total Pressure Coefficients, Velocity Ratios, and Static Pressure Coefficients in the Apertures of Model Configuration A

| Tap/Probe Number | Inlet | | | | Outlet | | | |
|---|---|---|---|---|---|---|---|---|
| | $\bar{C}_p$ open window | $C_{rms}$ | $(V_c/V_p)^2$ | $C_{p_s}$ | $\bar{C}_p$ open window | $C_{rms}$ | $(V_c/V_p)^2$ | $C_{p_s}$ |
| 2 | .270 | .094 | .084 | .186 | .165 | .080 | .204 | -.039 |
| 3 | .280 | .096 | .088 | .192 | .151 | .074 | .203 | -.052 |
| 4 | .264 | .093 | .088 | .176 | .156 | .070 | .205 | -.049 |
| 7 | .240 | .102 | .064 | .176 | .155 | .076 | .194 | -.039 |
| 8 | .243 | .098 | .065 | .178 | .191 | .085 | .171 | -.020 |
| 9 | .234 | .098 | .070 | .164 | .181 | .080 | .195 | -.014 |
| 12 | .208 | .081 | .042 | .166 | .182 | .078 | .203 | -.021 |
| 13 | .207 | .088 | .033 | .174 | .171 | .074 | .198 | -.027 |
| 14 | .203 | .080 | .048 | .155 | .171 | .069 | .209 | -.038 |
| Average | .235 | | .065 | .174 | .169 | | .198 | -.033 |

Table 3b. Total Pressure Coefficients, Velocity Ratios, and Static Pressure Coefficients in the Apertures of Model Configuration B

| Tap/Probe Number | Inlet | | | | Outlet | | | |
|---|---|---|---|---|---|---|---|---|
| | $\bar{C}_p$ open window | $C_{rms}$ | $(V_c/V_p)^2$ | $C_{p_s}$ | $\bar{C}_p$ open window | $C_{rms}$ | $(V_c/V_p)^2$ | $C_{p_s}$ |
| 2 | .264 | .097 | .236 | .028 | -.024 | .042 | .053 | -.077 |
| 3 | .267 | .099 | .220 | .047 | -.032 | .038 | .052 | -.084 |
| 4 | .269 | .092 | .234 | .035 | -.033 | .041 | .058 | -.091 |
| 7 | .242 | .099 | .207 | .035 | -.022 | .045 | .056 | -.058 |
| 8 | .233 | .100 | .194 | .039 | -.011 | .038 | .059 | -.070 |
| 9 | .221 | .088 | .213 | .008 | -.012 | .045 | .068 | -.080 |
| 12 | .185 | .093 | .198 | -.013 | .008 | .050 | .051 | -.043 |
| 13 | .176 | .097 | .168 | .008 | .005 | .047 | .060 | -.055 |
| 14 | .205 | .091 | .197 | .008 | .000 | .052 | .060 | -.060 |
| Average | .229 | | | | -.011 | | | |

Table 3c. Total Pressure Coefficients, Velocity Ratios, and Static Pressure Coefficients in the Apertures of Model Configuration C

| Tap/Probe Number | Inlet | | | | Outlet | | | |
|---|---|---|---|---|---|---|---|---|
| | $\bar{C}_p$ open window | $C_{rms}$ | $(V_c/V_p)^2$ | $C_{p_s}$ | $\bar{C}_p$ open window | $C_{rms}$ | $(V_c/V_p)^2$ | $C_{p_s}$ |
| 1 | .281 | .104 | | | | | | |
| 2 | .281 | .107 | .136 | .145 | .057 | .052 | .122 | -.065 |
| 3 | .286 | .103 | .157 | .129 | .076 | .057 | .166 | -.090 |
| 4 | .279 | .097 | .165 | .114 | .084 | .060 | .224 | -.140 |
| 6 | .249 | .095 | | | | | | |
| 7 | .236 | .088 | .113 | .123 | .056 | .048 | .086 | -.030 |
| 8 | .266 | .097 | .126 | .140 | .072 | .056 | .106 | -.034 |
| 9 | .238 | .094 | .138 | .100 | .084 | .057 | .182 | -.098 |
| 11 | .223 | .084 | | | | | | |
| 12 | .224 | .095 | .092 | .132 | .062 | .056 | .114 | -.052 |
| 13 | .200 | .092 | .077 | .123 | .058 | .061 | .155 | -.097 |
| 14 | .213 | .087 | .098 | .115 | .073 | .057 | .210 | -.137 |
| Average | .247 | | | | .069 | | | |

Table 4a. Velocity Ratios and Turbulence Intensities Measured Near the Apertures of Model Configuration A

| Inlet | | | | | |
|---|---|---|---|---|---|
| Probe Location | Vert. inside $V/V_p$ | Vert. inside TI(%) | Omnidirectional-inside $V_2/V_p$ | Omnidirectional-outside $V_1/V_p$ | Calculated $V/V_p$ at Total Pressure Location |
| 2 | .302 | 31.7 | .304 | .251 | .289 |
| 3 | .304 | 28.3 | .309 | .263 | .296 |
| 4 | .312 | 32.5 | .310 | .260 | .296 |
| 7 | .262 | 37.3 | .259 | .234 | .252 |
| 8 | .249 | 35.1 | .256 | .251 | .254 |
| 9 | .270 | 39.0 | .269 | .249 | .264 |
| 12 | .197 | 45.9 | .209 | .195 | .205 |
| 13 | .181 | 46.5 | .180 | .183 | .181 |
| 14 | .223 | 48.4 | .224 | .201 | .218 |
| Average | | | .258 | .232 | |

| Outlet | | | | | |
|---|---|---|---|---|---|
| Probe Location | Vert. inside $V/V_p$ | Vert. inside TI(%) | Omnidirectional-inside $V_1/V_p$ | Omnidirectional-outside $V_2/V_p$ | Calculated $V/V_p$ at Total Pressure Position |
| 2 | .351 | 17.9 | .348 | .491 | .452 |
| 3 | .334 | 18.0 | .357 | .487 | .451 |
| 4 | .339 | 17.4 | .352 | .491 | .453 |
| 7 | .338 | 17.5 | .342 | .478 | .440 |
| 8 | .341 | 18.2 | .340 | .443 | .414 |
| 9 | .334 | 17.2 | .348 | .478 | .442 |
| 12 | .303 | 19.6 | .341 | .493 | .451 |
| 13 | .292 | 21.0 | .345 | .484 | .445 |
| 14 | .288 | 18.9 | .341 | .500 | .457 |
| Average | | | .346 | .483 | .445 |

Table 4b. Velocity Ratios and Turbulence Intensities Measured Near the Apertures of Model Configuration B

| Inlet | | | | | |
|---|---|---|---|---|---|
| Probe Location | Vert. inside $V/V_p$ | Vert. inside TI(%) | Omnidirectional-inside $V_2/V_p$ | Omnidirectional-outside $V_1/V_p$ | Calculated $V/V_p$ at Total Pressure Location |
| 2 | .535 | 16.1 | .536 | .357 | .486 |
| 3 | .525 | 16.7 | .501 | .384 | .469 |
| 4 | .562 | 18.1 | .528 | .368 | .484 |
| 7 | .509 | 19.0 | .493 | .358 | .455 |
| 8 | .471 | 20.2 | .467 | .372 | .441 |
| 9 | .523 | 18.9 | .498 | .363 | .461 |
| 12 | .478 | 21.5 | .504 | .292 | .445 |
| 13 | .423 | 26.1 | .457 | .287 | .410 |
| 14 | .496 | 21.9 | .500 | .298 | .444 |
| Average | | | .498 | .342 | |

| Outlet | | | | | |
|---|---|---|---|---|---|
| Probe Location | Vert. inside $V/V_p$ | Vert. inside TI(%) | Omnidirectional-inside $V_1/V_p$ | Omnidirectional-outside $V_2/V_p$ | Calculated $V/V_p$ at Total Pressure Location |
| 2 | .183 | 33.7 | .192 | .245 | .230 |
| 3 | .186 | 34.6 | .192 | .240 | .227 |
| 4 | .187 | 33.8 | .198 | .257 | .241 |
| 7 | .199 | 31.9 | .202 | .251 | .237 |
| 8 | .207 | 32.3 | .212 | .255 | .243 |
| 9 | .201 | 32.3 | .225 | .275 | .261 |
| 12 | .196 | 32.7 | .200 | .234 | .225 |
| 13 | .210 | 31.4 | .200 | .261 | .244 |
| 14 | .222 | 32.1 | .215 | .255 | .244 |
| Average | | | .204 | .253 | |

Table 4c. Velocity Ratios and Turbulence Intensities Measured Near the Apertures of Model Configuration C

| Inlet | | | | | |
|---|---|---|---|---|---|
| Probe Location | Vert. inside $V/V_p$ | Vert. inside TI(%) | Omnidirectional-inside $V_2/V_p$ | Omnidirectional-outside $V_1/V_p$ | Calculated $V/V_p$ at Total Pressure Location |
| 2 | .422 | 25.4 | .392 | .309 | .369 |
| 3 | .439 | 20.5 | .416 | .347 | .396 |
| 4 | .444 | 22.8 | .433 | .337 | .406 |
| 7 | .341 | 31.8 | .351 | .297 | .336 |
| 8 | .362 | 24.7 | .369 | .318 | .355 |
| 9 | .388 | 25.6 | .392 | .322 | .372 |
| 12 | .304 | 35.6 | .328 | .236 | .303 |
| 13 | .291 | 34.3 | .288 | .248 | .277 |
| 14 | .353 | 31.8 | .334 | .257 | .313 |
| Average | | | .367 | .297 | |

| Outlet | | | | | |
|---|---|---|---|---|---|
| Probe Location | Vert. inside $V/V_p$ | Vert. inside TI(%) | Omnidirectional-inside $V_1/V_p$ | Omnidirectional-outside $V_2/V_p$ | Calculated $V/V_p$ at Total Pressure Position |
| 2 | .264 | 32.0 | .273 | .378 | .349 |
| 3 | .336 | 23.8 | .325 | .438 | .407 |
| 4 | .398 | 19.4 | .389 | .506 | .473 |
| 7 | .250 | 33.6 | .235 | .316 | .293 |
| 8 | .308 | 27.3 | .285 | .342 | .326 |
| 9 | .414 | 19.5 | .373 | .448 | .427 |
| 12 | .240 | 30.5 | .250 | .370 | .337 |
| 13 | .299 | 25.1 | .309 | .427 | .394 |
| 14 | .369 | 21.1 | .387 | .486 | .459 |
| Average | | | .314 | .412 | |

Table 5a. Velocity Ratios and Turbulence Intensities Measured Inside Model Configuration A

| Point Number | X/L | Y/L | Z/H | Omnidirectional Probe V/V$_p$ | Vertical Probe V/V$_p$ | Vertical Probe TI(%) |
|---|---|---|---|---|---|---|
| 1 | .5 | .5 | .5 | .095 | .105 | 49.4 |
| 2 | .5 | .5 | 1.* | .064 | .052 | 44.8 |
| 3 | .5 | 1.* | .5 | .065 | .064 | 36.5 |
| 4 | .1 | .9 | .5 | .053 | .053 | 36.6 |
| 5 | .9 | .9 | .5 | .063 | .066 | 38.8 |
| 6 | .25 | .42 | .5 | .158 | .151 | 54.8 |
| 7 | .75 | .42 | .5 | .095 | .094 | 37.2 |
| 8 | .5 | .5 | 0 | .122 | .138 | 56.3 |
| 9 | .1 | .9 | 0 | .042 | .043 | 46.7 |

Table 5b. Velocity Ratios and Turbulence Intensities Measured Inside Model Configuration B

| Point Number | X/L | Y/L | Z/H | Omnidirectional Probe V/V$_p$ | Vertical Probe V/V$_p$ | Vertical Probe TI(%) |
|---|---|---|---|---|---|---|
| 1 | .5 | .5 | .5 | .293 | .300 | 50.6 |
| 2 | .5 | .5 | 1.* | .145 | .135 | 53.6 |
| 3 | .5 | 1.* | .5 | .092 | .073 | 39.0 |
| 4 | .1 | .9 | .5 | .062 | .058 | 68.8 |
| 5 | .9 | .9 | .5 | .086 | .091 | 42.9 |
| 6 | .25 | .42 | .5 | .223 | .220 | 68.7 |
| 7 | .75 | .42 | .5 | .185 | .182 | 53.1 |
| 8 | .5 | .5 | 0 | .265 | .269 | 45.0 |
| 9 | .1 | .9 | 0 | .061 | .067 | 45.2 |

Table 5c. Velocity Ratios and Turbulence Intensities Measured Inside Model Configuration C

| Point Number | X/L | Y/L | Z/H | Omnidirectional Probe V/V$_p$ | Vertical Probe V/V$_p$ | Vertical Probe TI(%) |
|---|---|---|---|---|---|---|
| 1 | .5 | .5 | .5 | .204 | .222 | 49.2 |
| 2 | .5 | .5 | 1.* | .185 | .186 | 49.8 |
| 3 | .5 | 1.* | .5 | .180 | .090 | 29.3 |
| 4 | 1.* | .5 | .5 | .160 | .165 | 42.1 |
| 5 | .67 | .67 | .5 | .099 | .095 | 47.3 |
| 6 | .33 | .33 | .5 | .191 | .191 | 56.5 |
| 7 | 1.* | 1.* | .5 | .059 | .055 | 32.6 |
| 8 | .33 | .67 | .5 | .110 | .117 | 39.0 |
| 9 | .5 | .5 | 0 | .168 | .175 | 49.6 |

*Probe located ~3.175 mm from surface

FIGURES

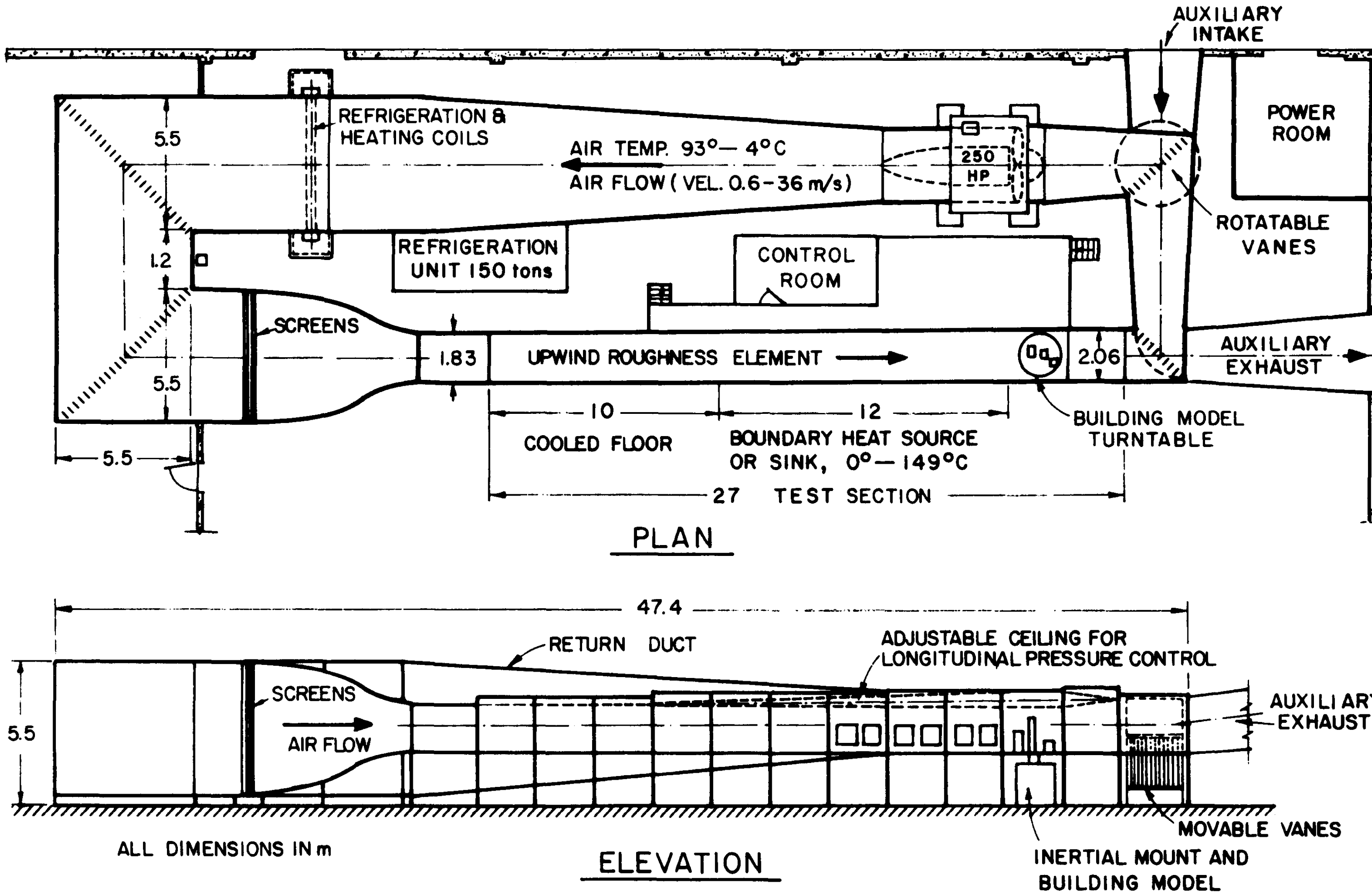


Figure 1. Meteorological Wind Tunnel, Fluid Dynamics and Diffusion Laboratory, Colorado State University

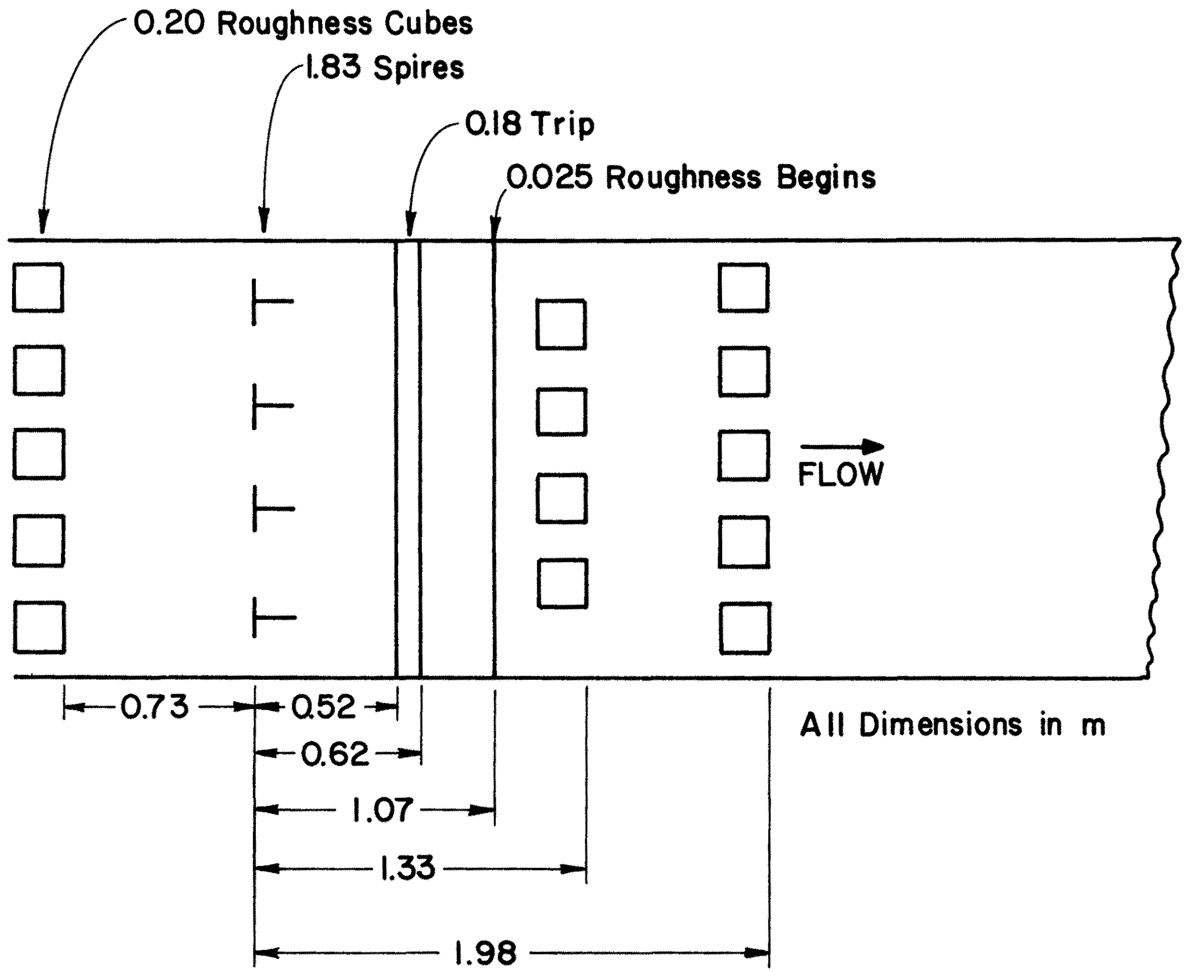


Figure 2. Wind-Tunnel Entrance Configuration for the Study.

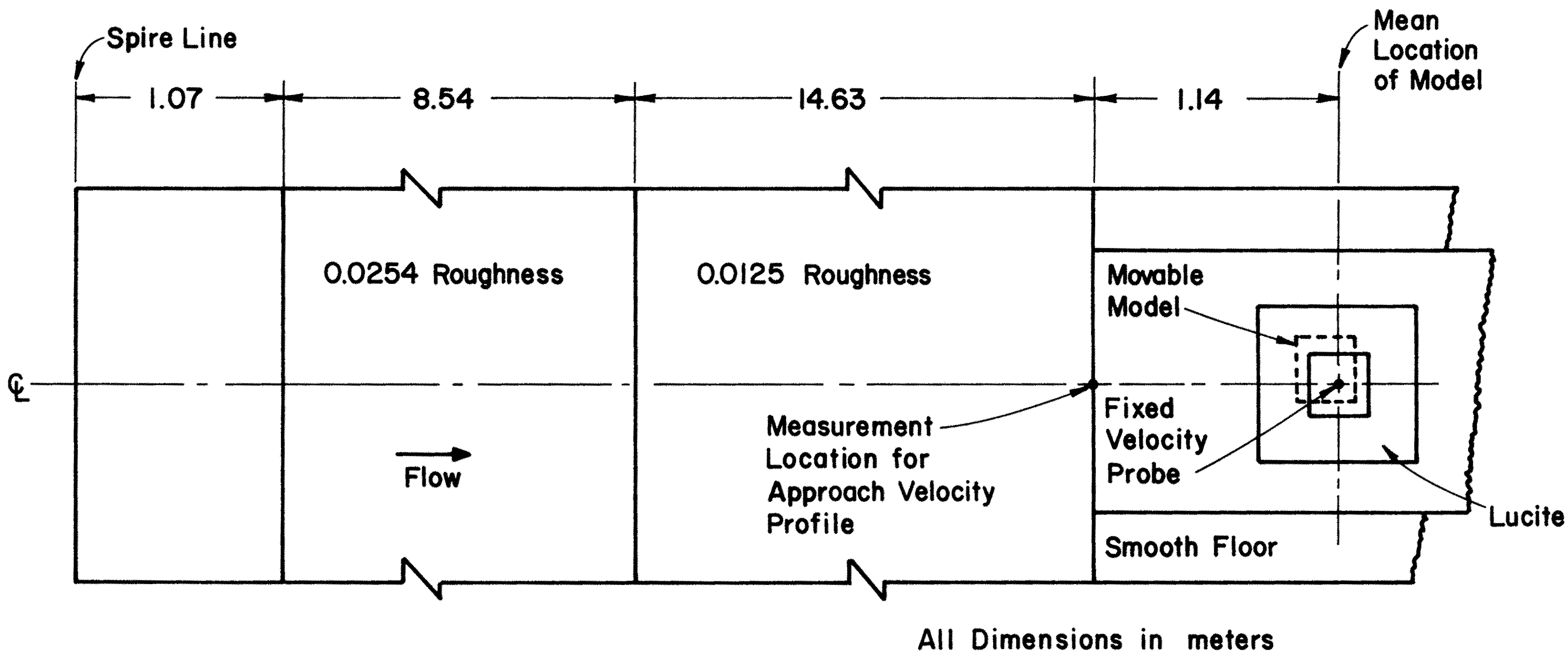


Figure 3. Wind-Tunnel Test Section Configuration for the Study.

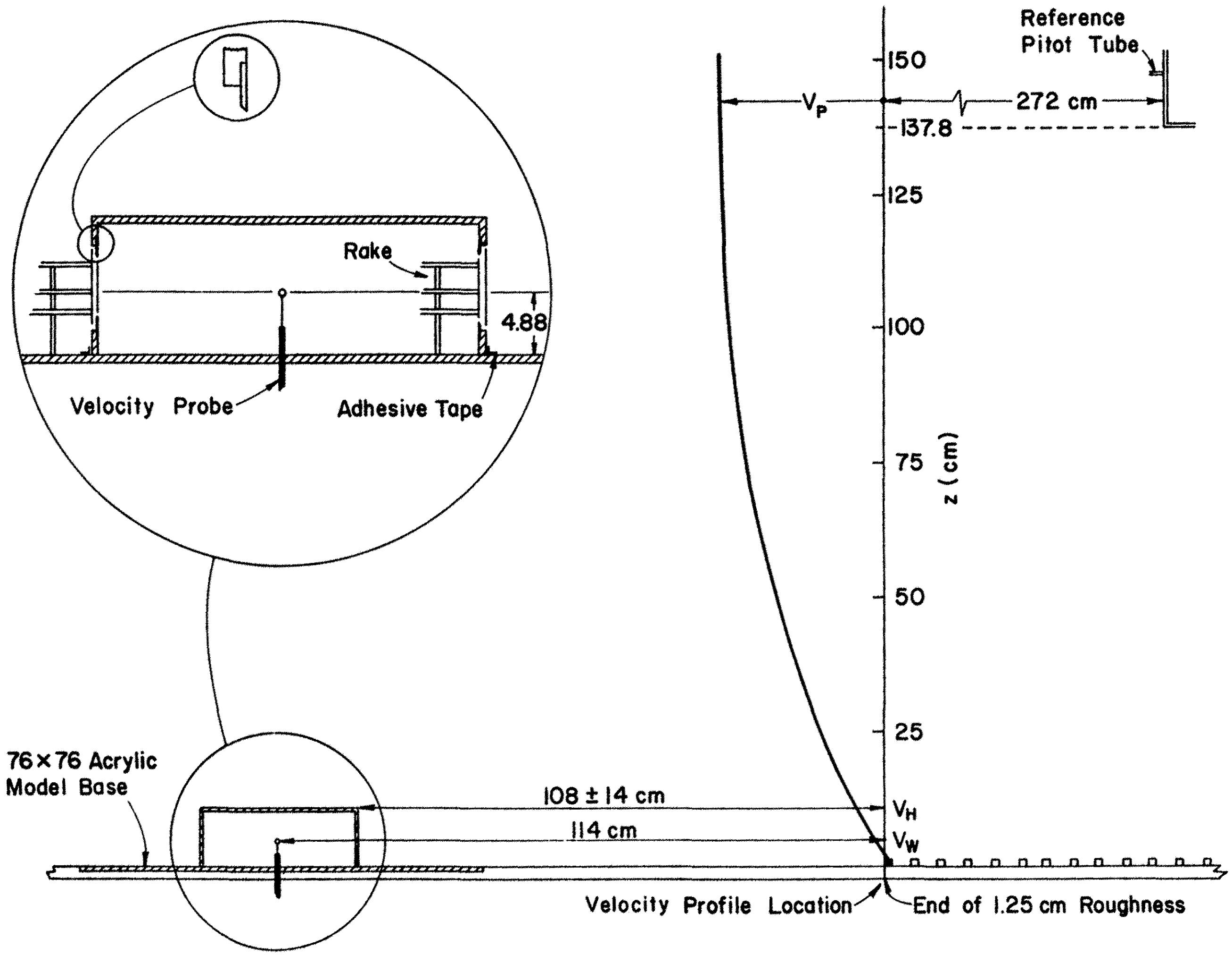


Figure 4. Wind-Tunnel Model Location for the Study.

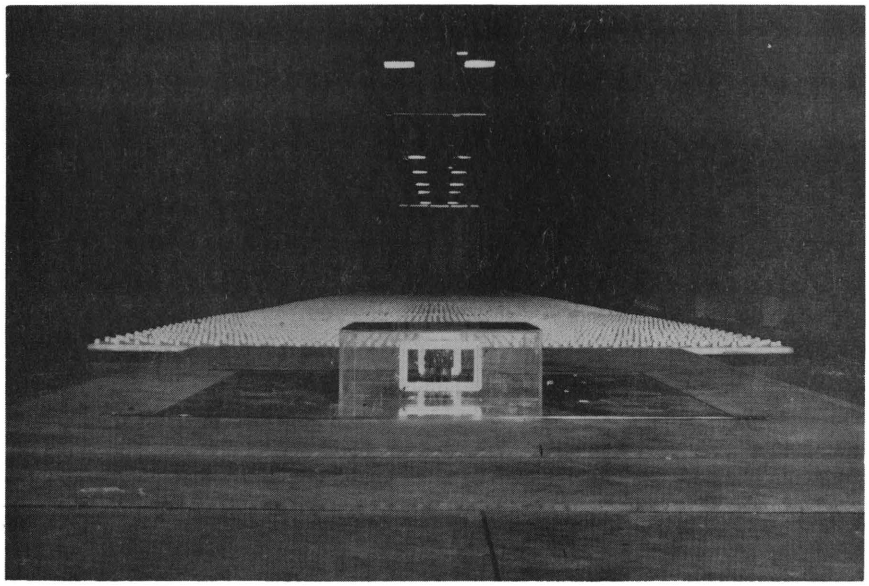

Figure 5. Model Configuration B in the Wind-Tunnel Looking Upwind

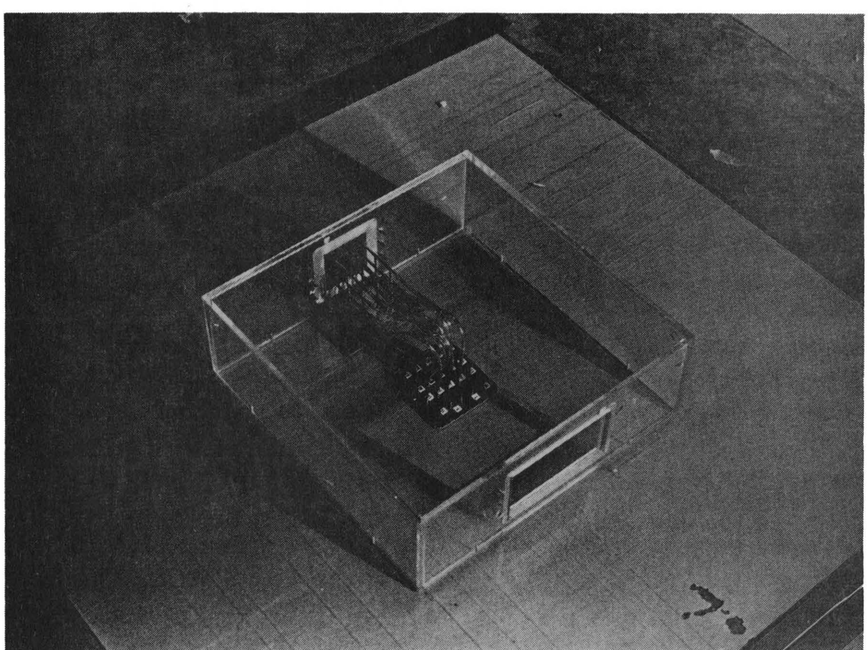

Figure 6. Model Configuration B in the Wind-Tunnel During Pressure Measurements

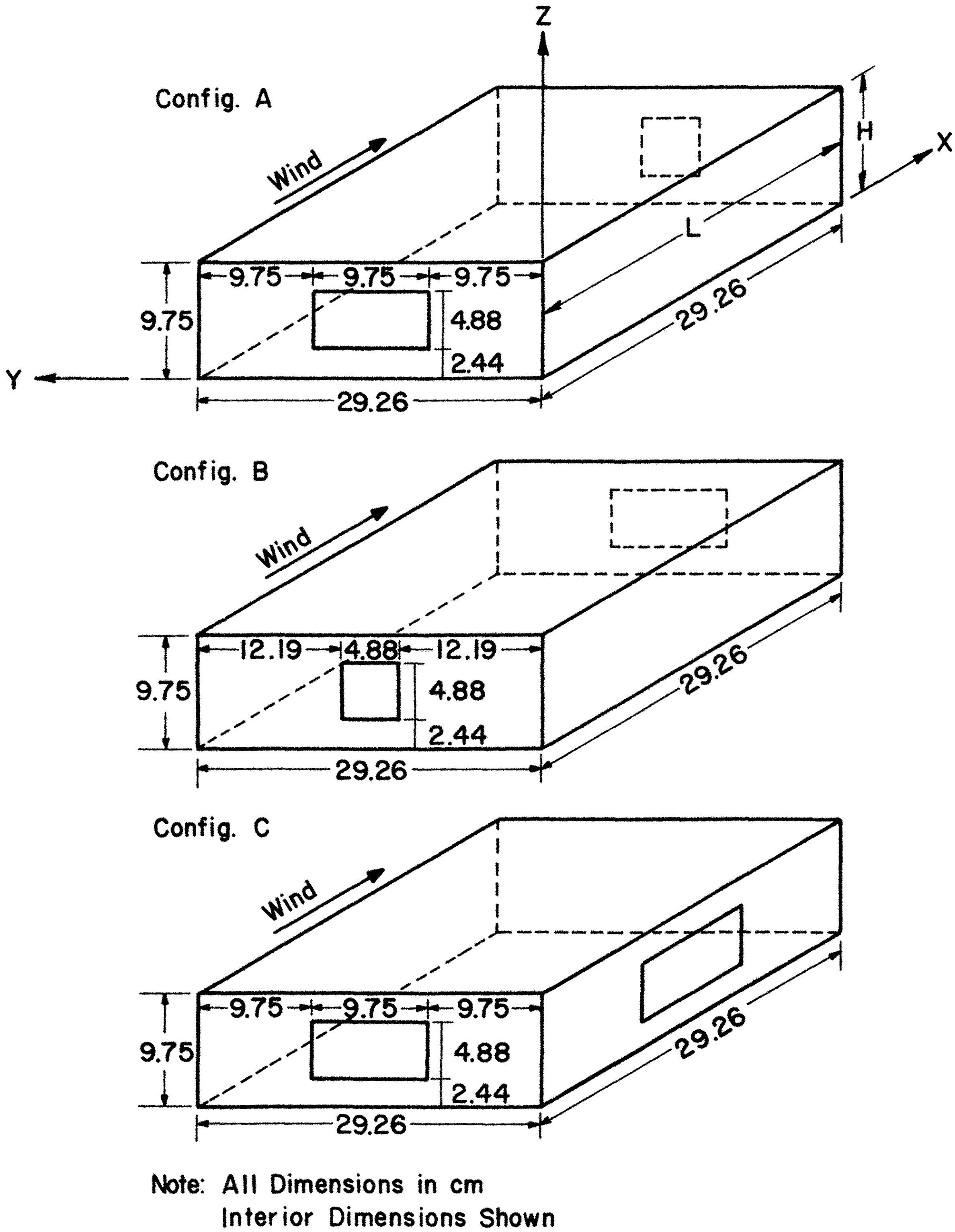


Figure 7. Interior Dimensions of the Three Model Configurations.

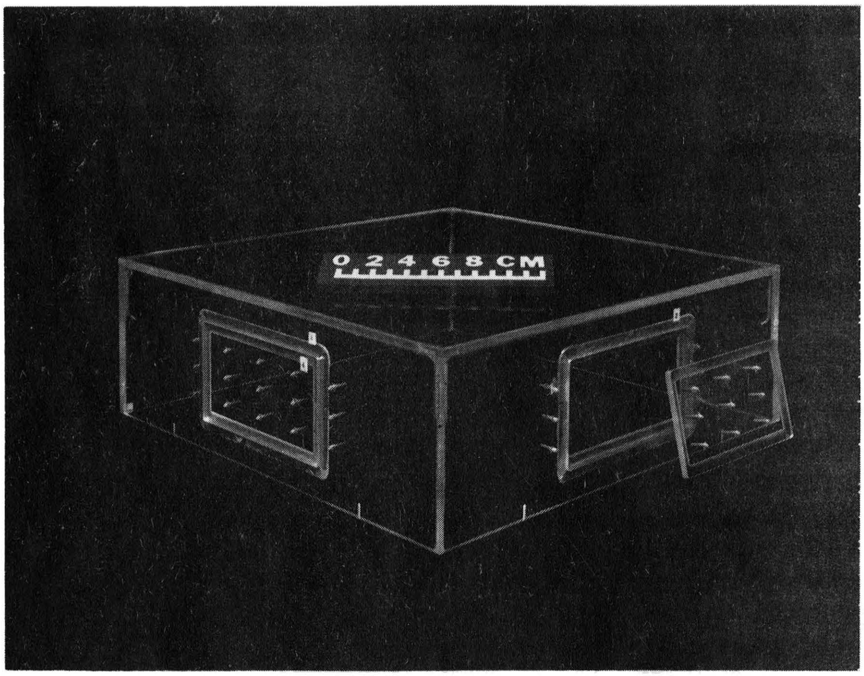


(a)

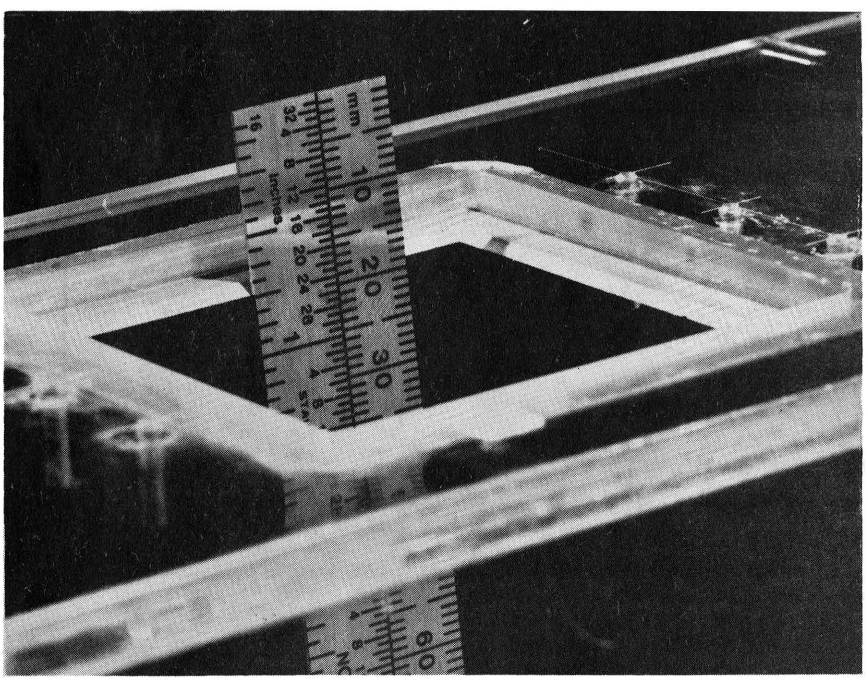

(b)

Figure 8. Photographs of Model Configuration C Depicting:
(a) Aperture Closures and Pressure Ports
(b) Detailed Construction of Apertures

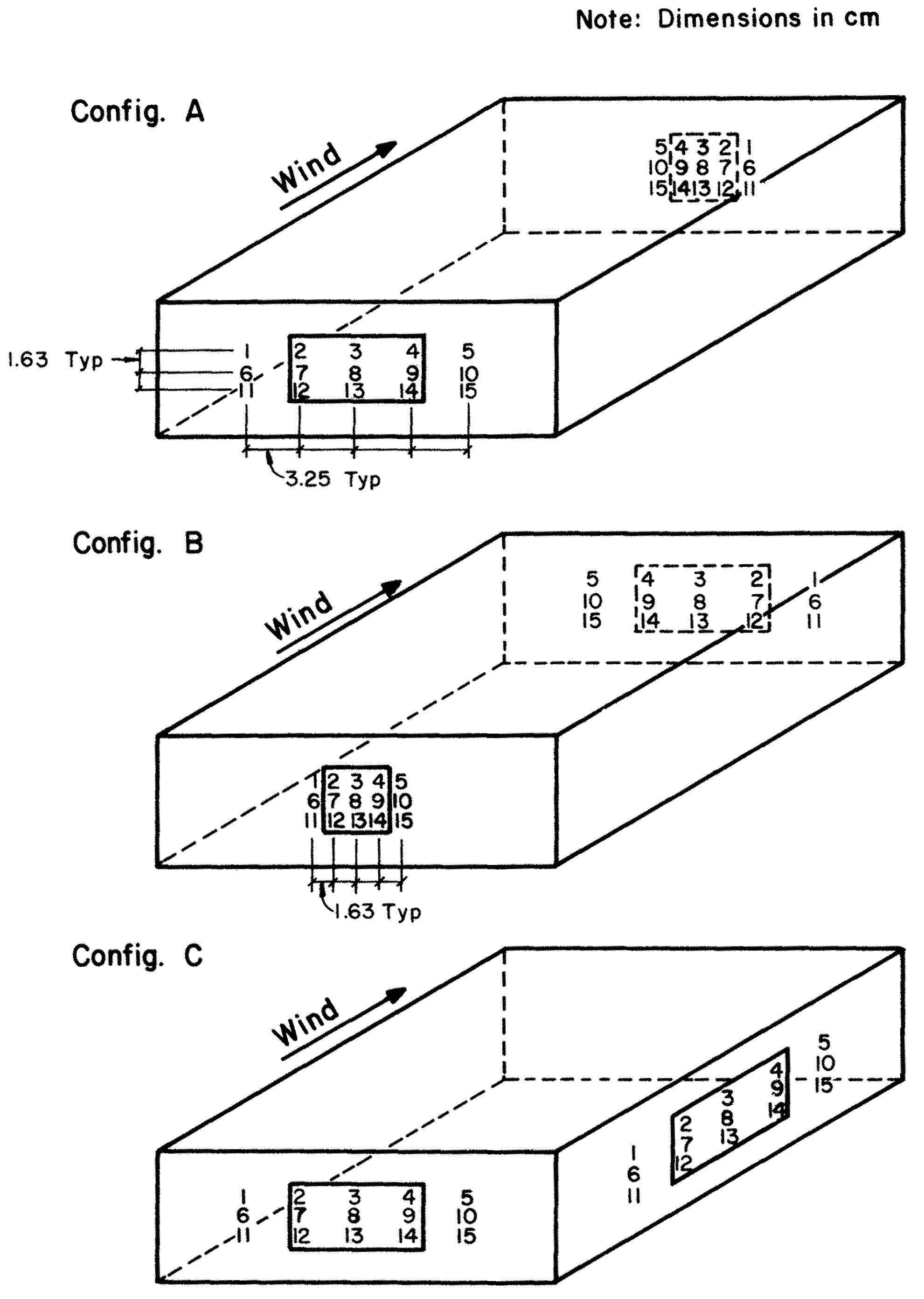


Figure 9. Location and Identification of Measurement Positions at the Apertures of the Three Model Configurations.

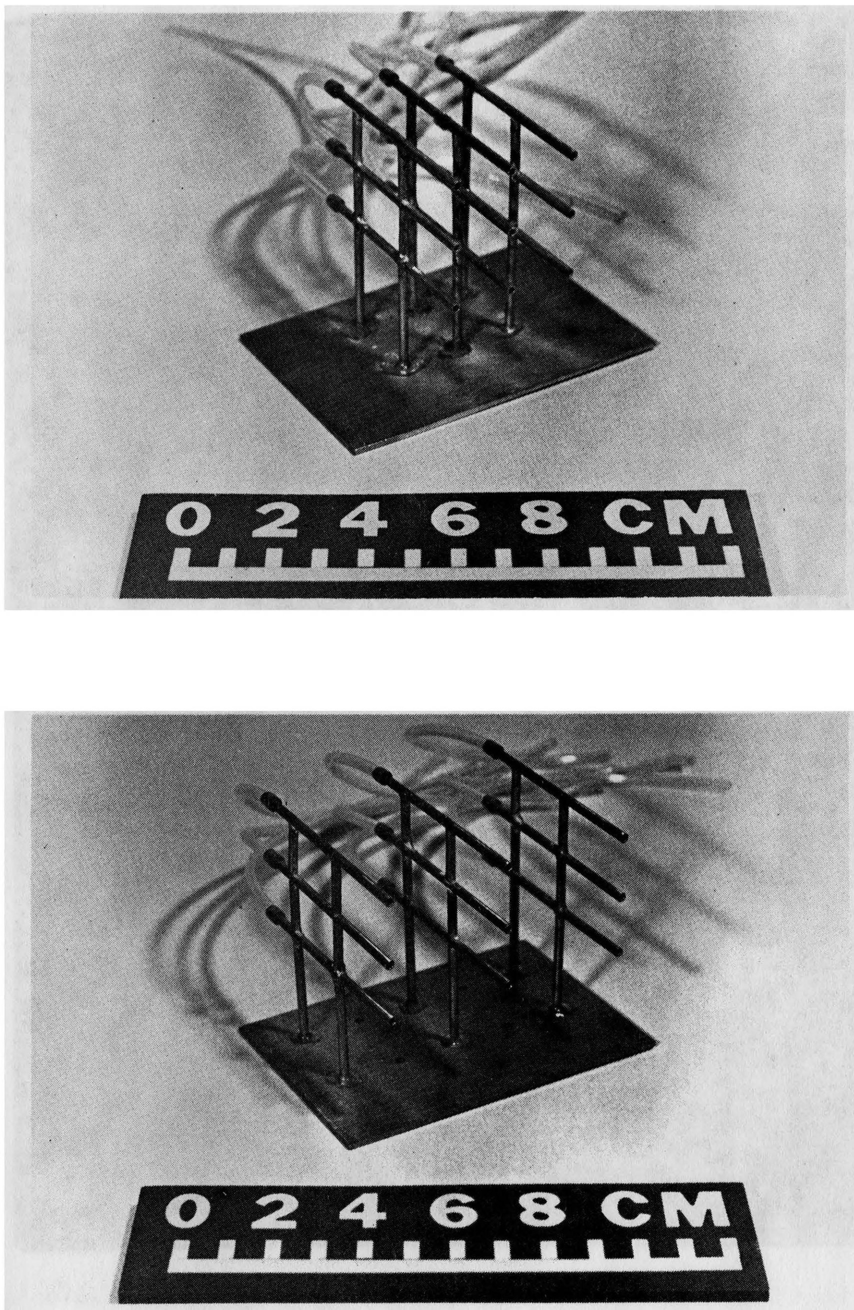


Figure 10. Rakes Used to Measure Total Pressures at the Apertures

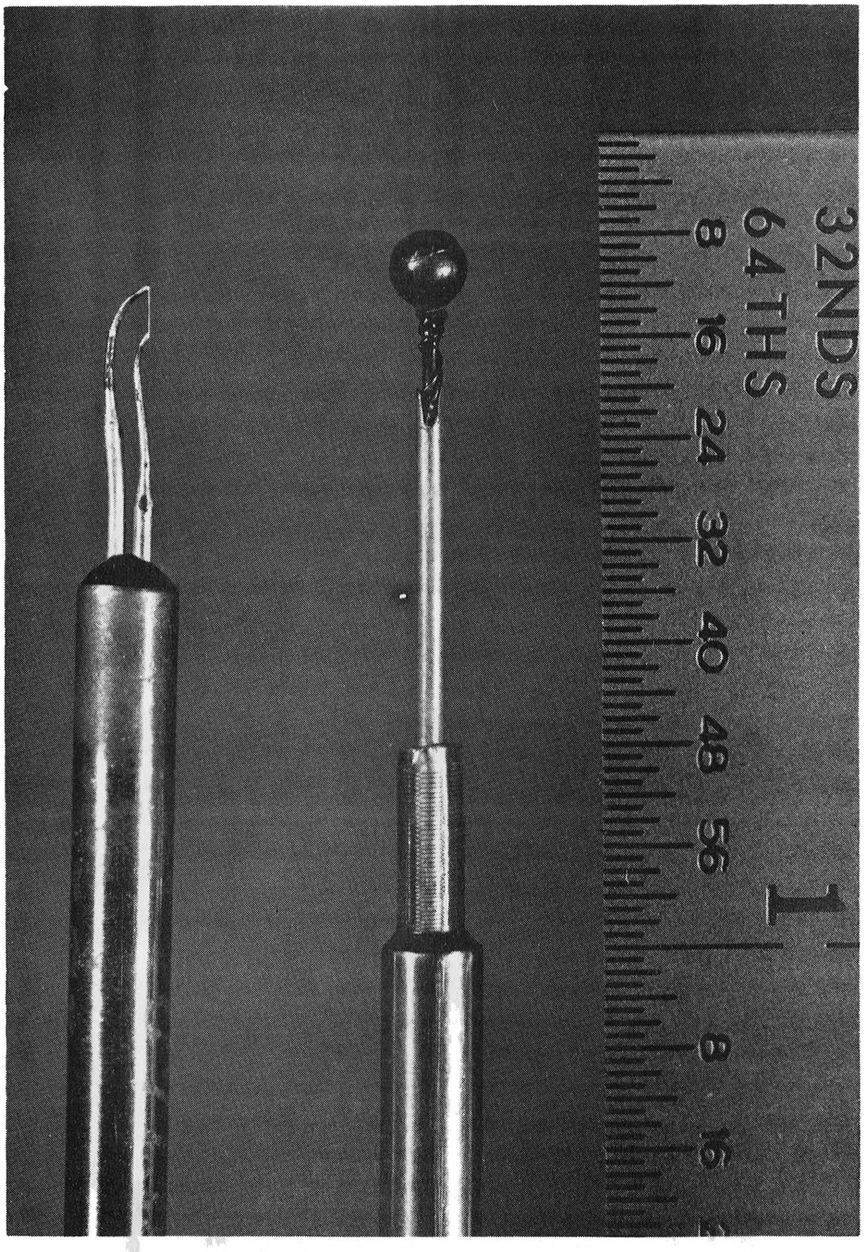


Figure 11. Comparison of the Omni-directional and Vertical Hot-film Probes Used to Measure Velocity and Turbulence

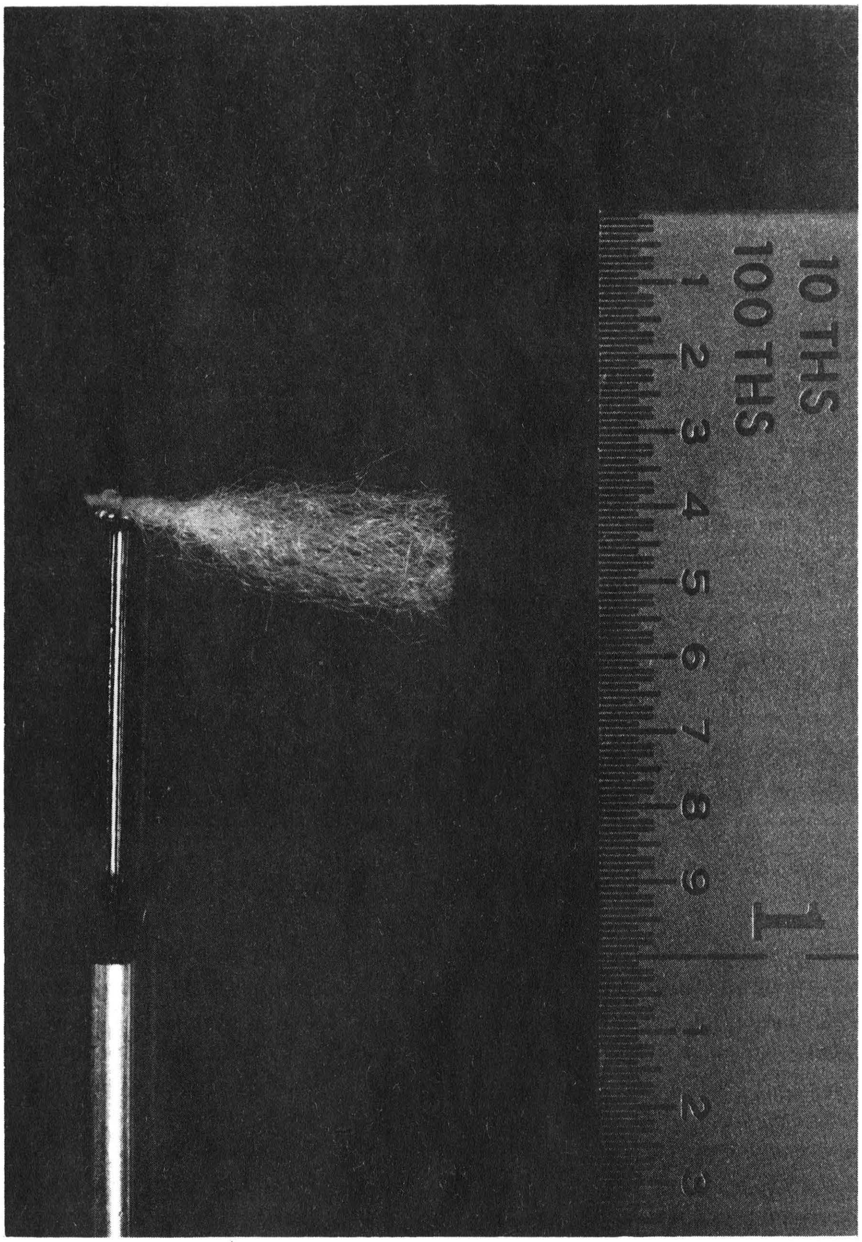


Figure 12. Close-up View of Typical Cotton Tuft Used in Flow Visualization Study

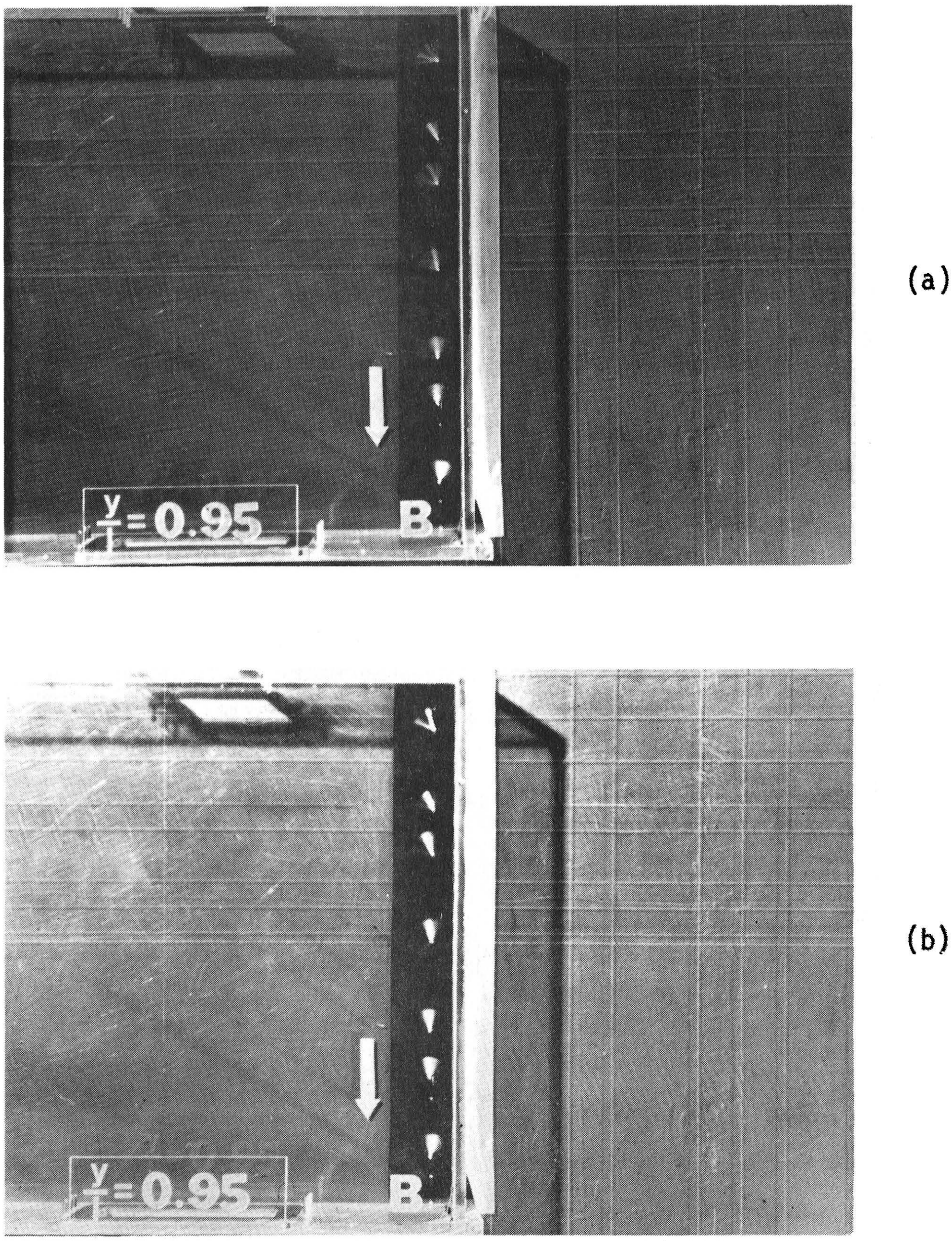


Figure 13. One-second Exposures of a Longitudinal Row of Tufts at Z/H = 0.5 and Y/L = 0.95, for Configuration B (Note: The nearly uniform upwind alignment of the tufts caused by the simple elongated vortex created by this configuration.)

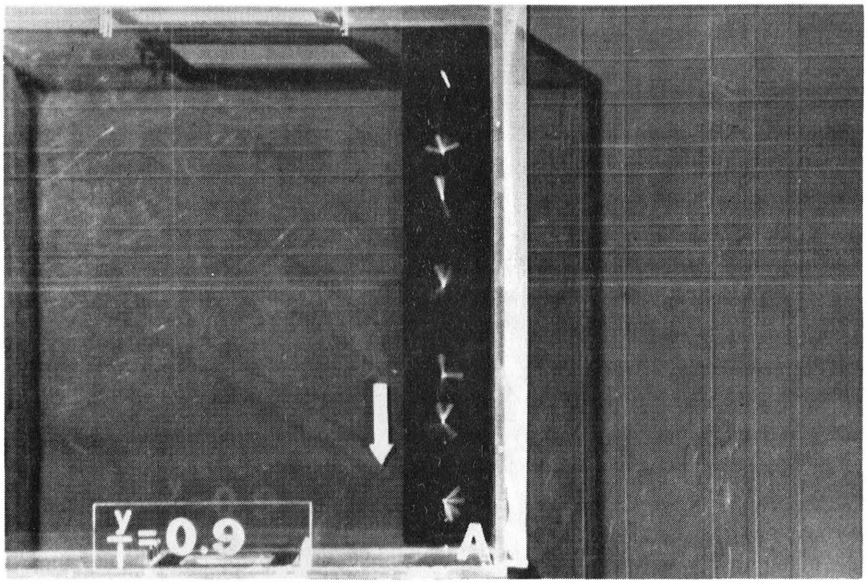


(a)

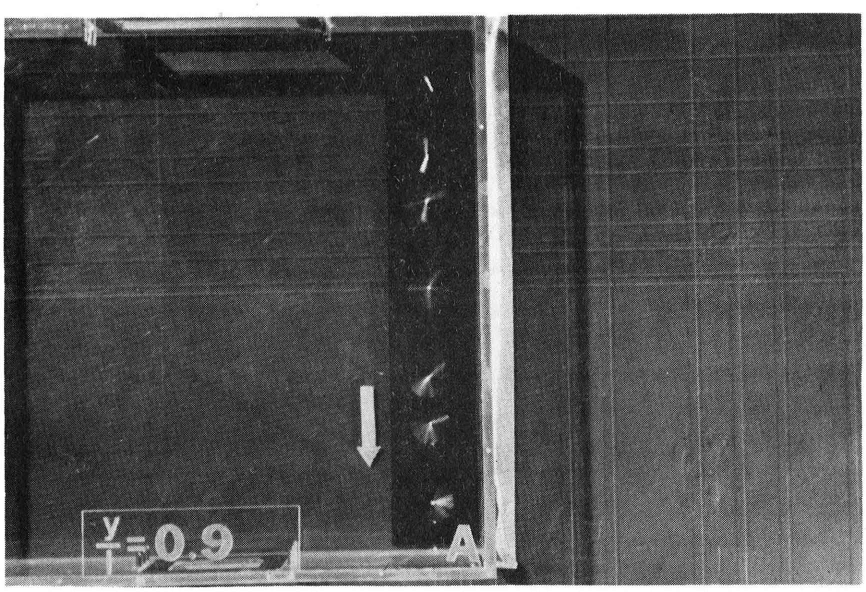


(b)

Figure 14. One-second Exposures of a Longitudinal Row of Tufts at Z/H = 0.5 and Y/L = 0.90, for Configuration A

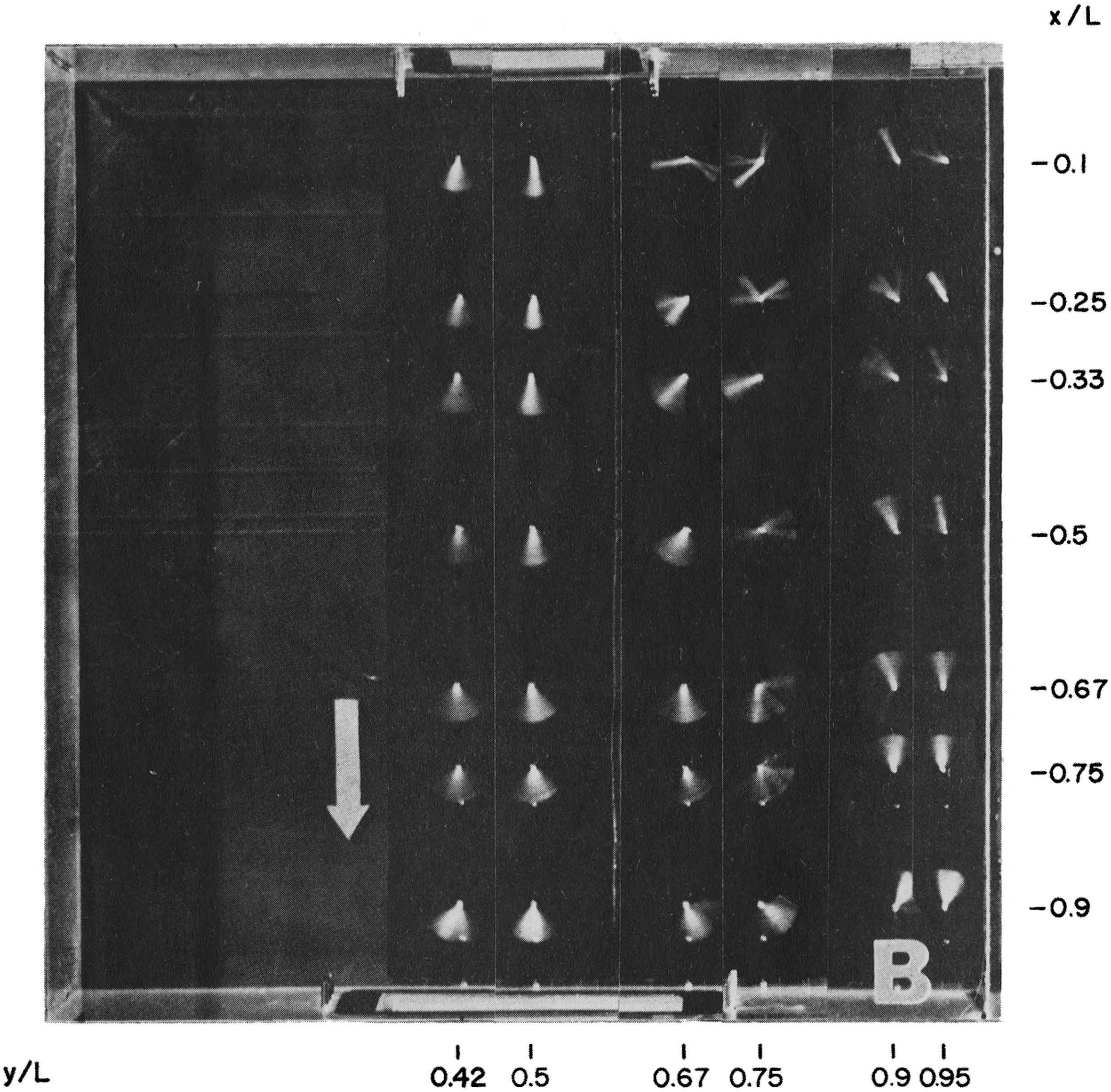
x/L
−0.1
−0.25
−0.33
−0.5
−0.67
−0.75
−0.9
B
y/L
0.42
0.5
0.67
0.75
0.9
0.95

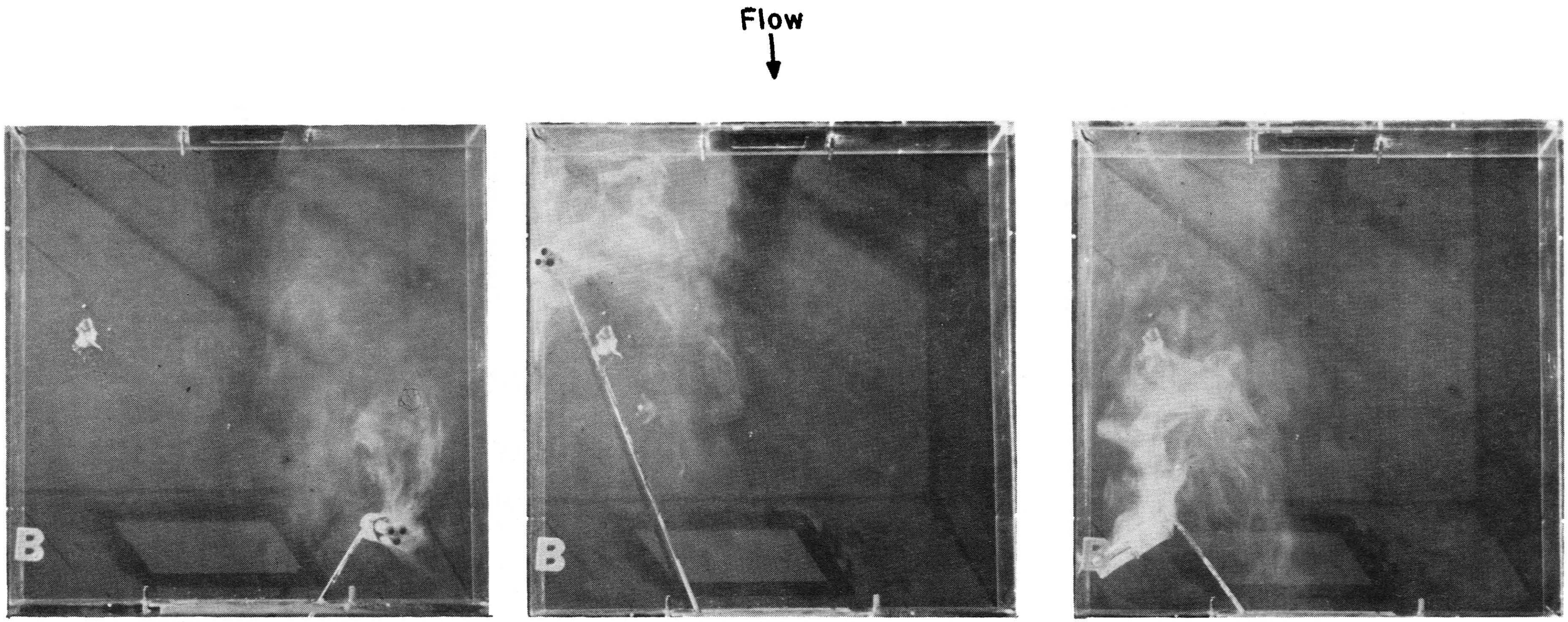


(a) (b) (c)

Figure 16. Flow Visualization for Configuration B Using Smoke.

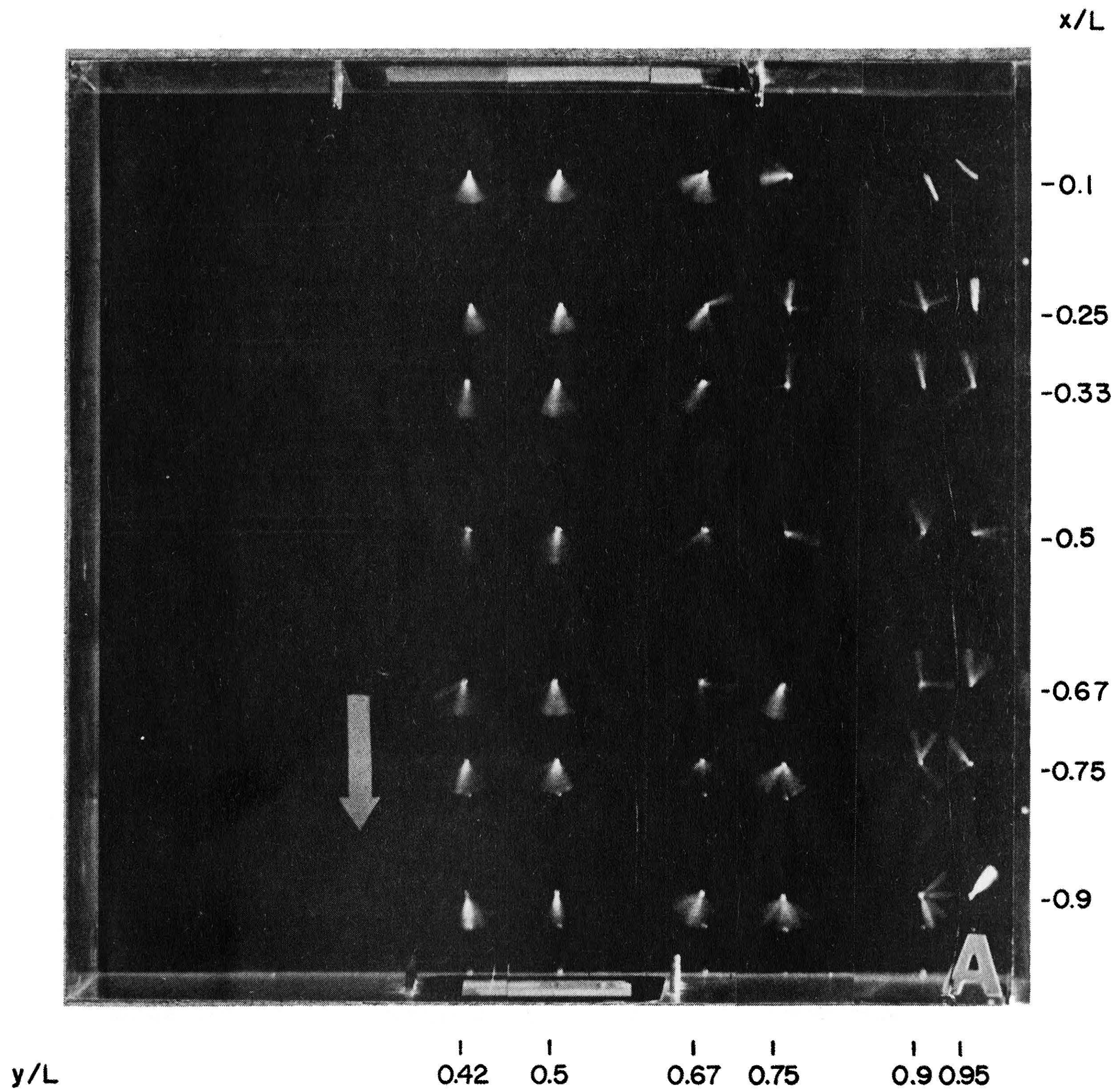


Figure 17. Orientation of the Tufts at Z/H = 0.5 in Configuration A

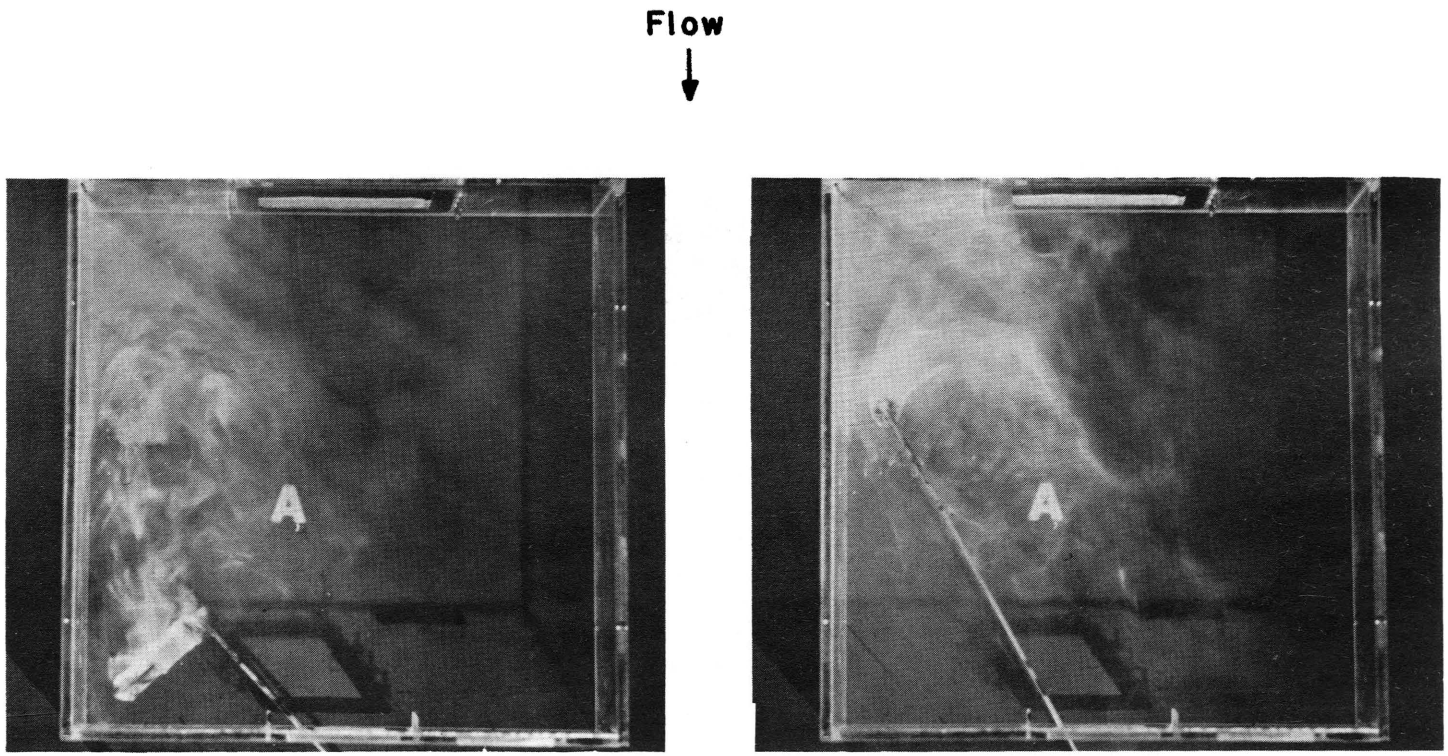


Figure 18. Flow Visualization for Configuration A Using Smoke.

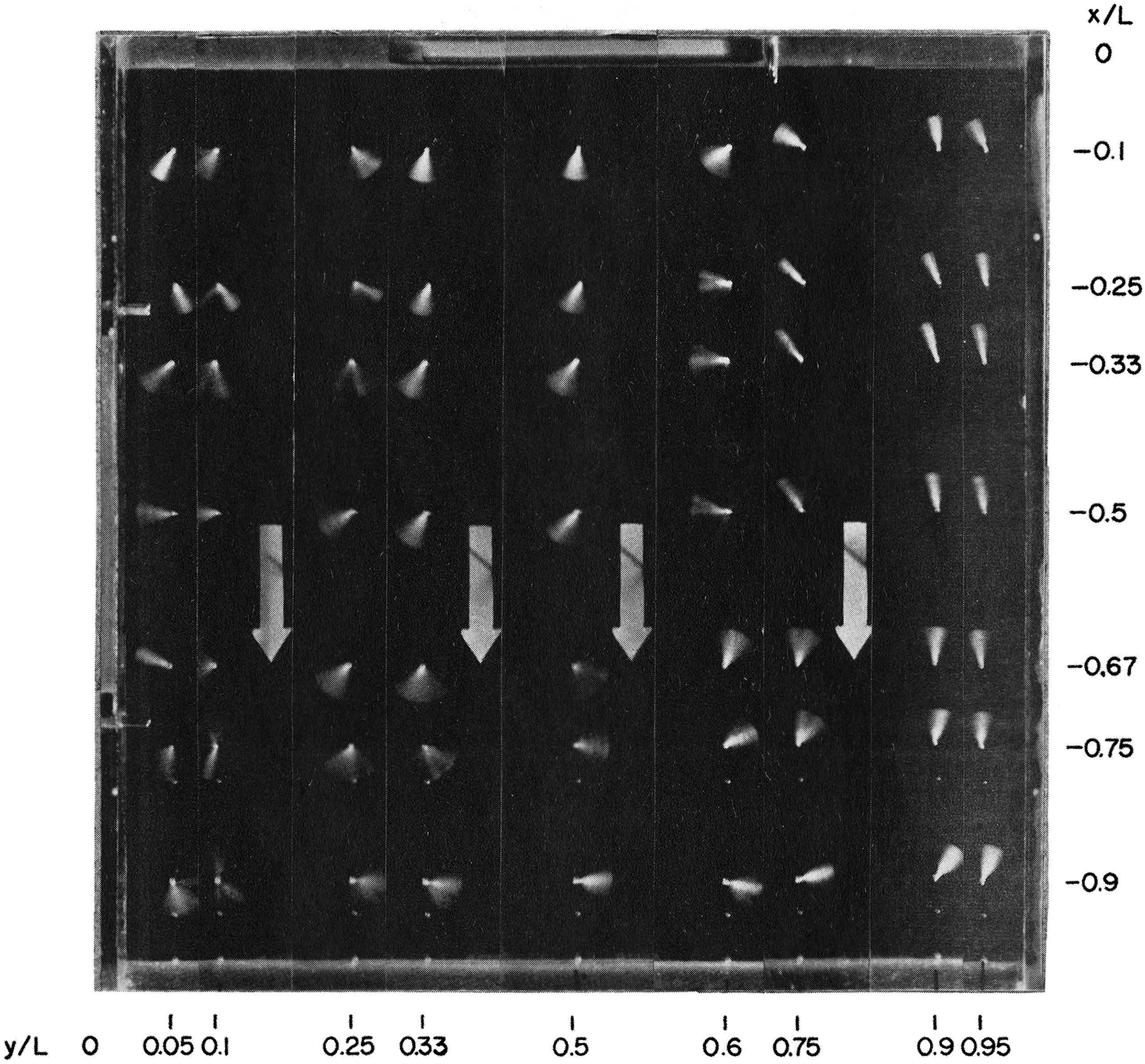


Figure 19. Orientation of the Tufts at Z/H = 0.5 in Configuration C

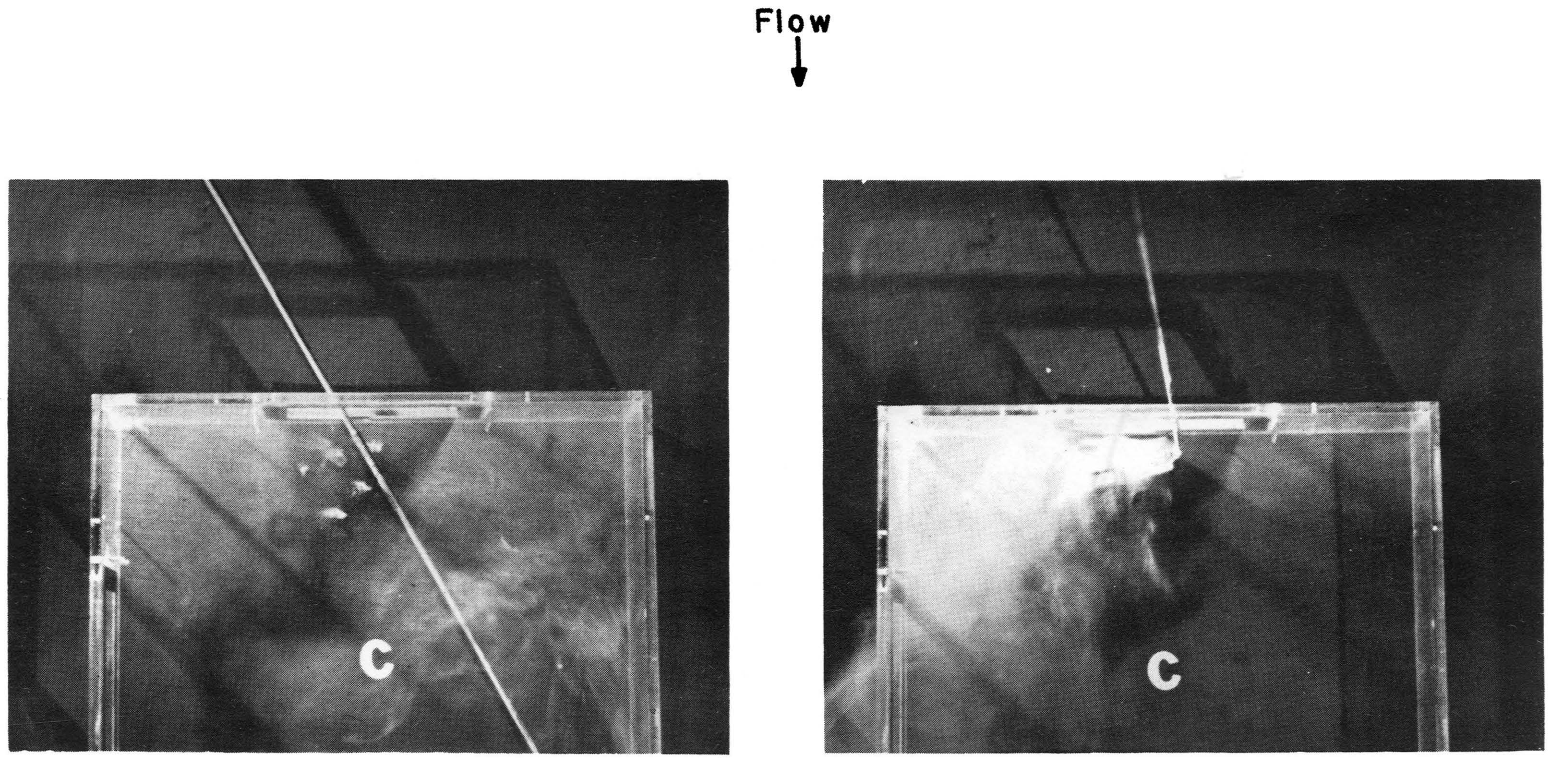


Figure 20. Flow Visualization of Configuration C with Smoke.

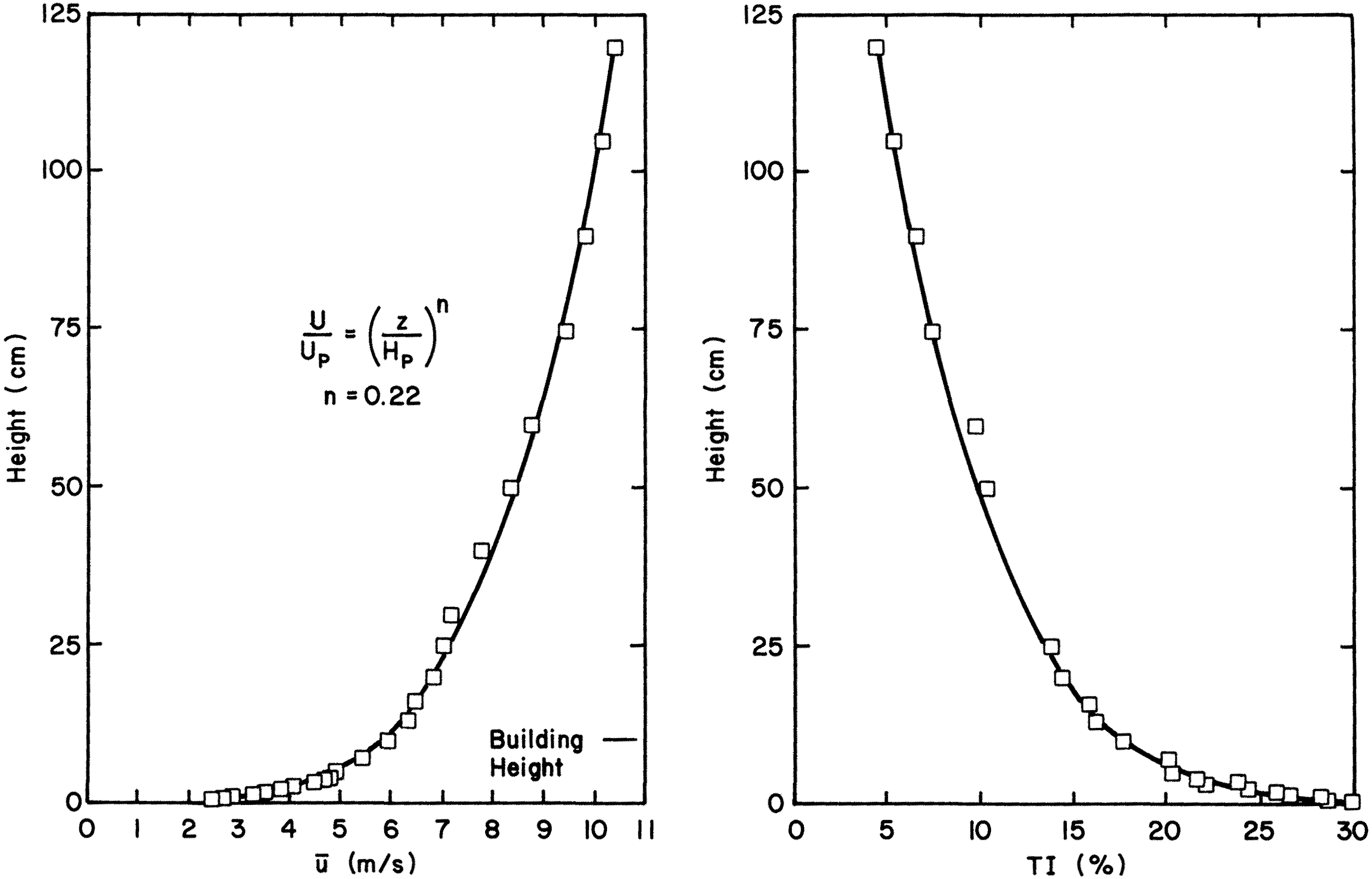


Figure 21. Mean Velocity and Turbulence Intensity Profiles above the Roughness in the Approach Flow.

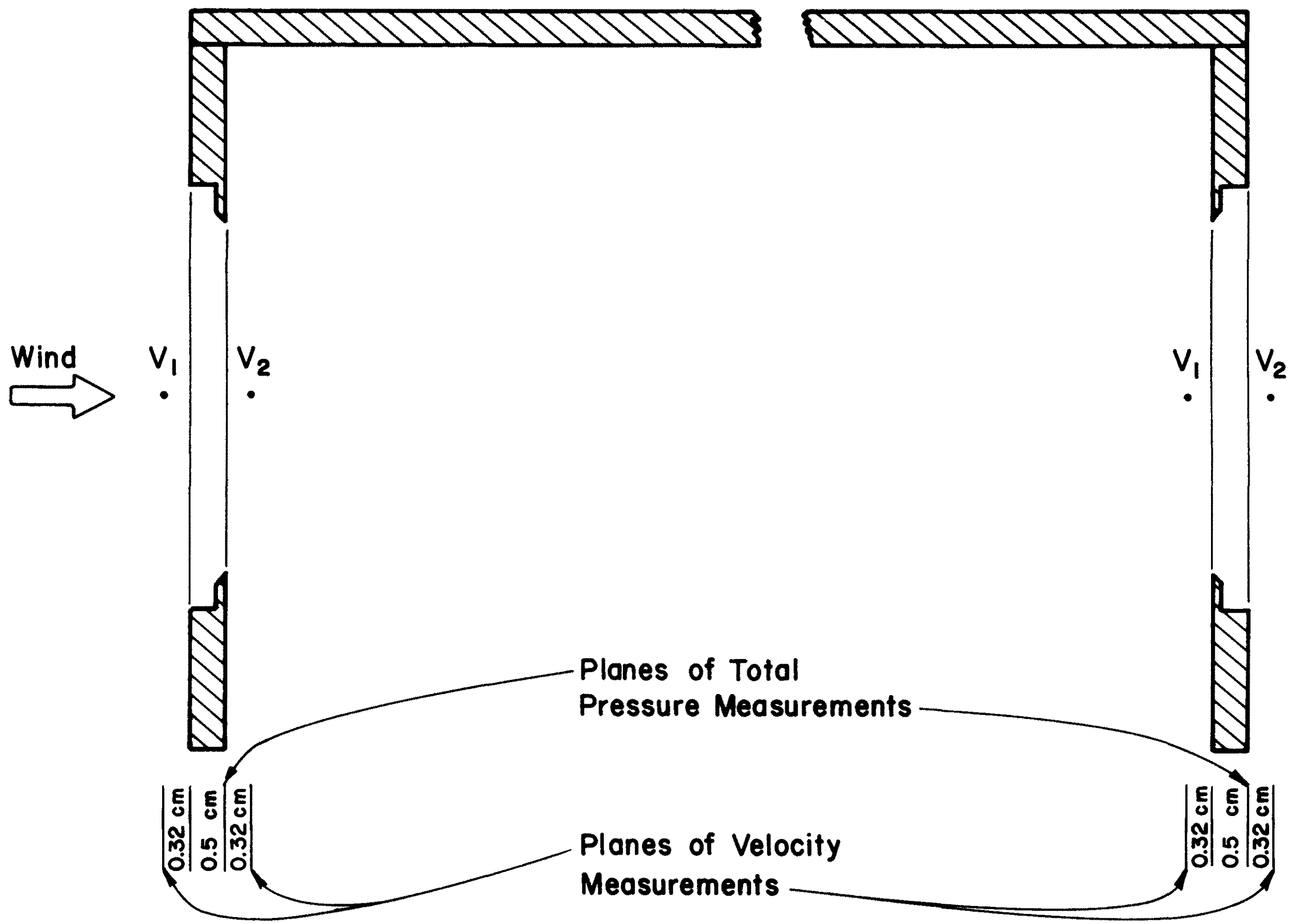


Figure 22. Location of Velocity Probes and Total Pressure Rakes Near the Open Windows.

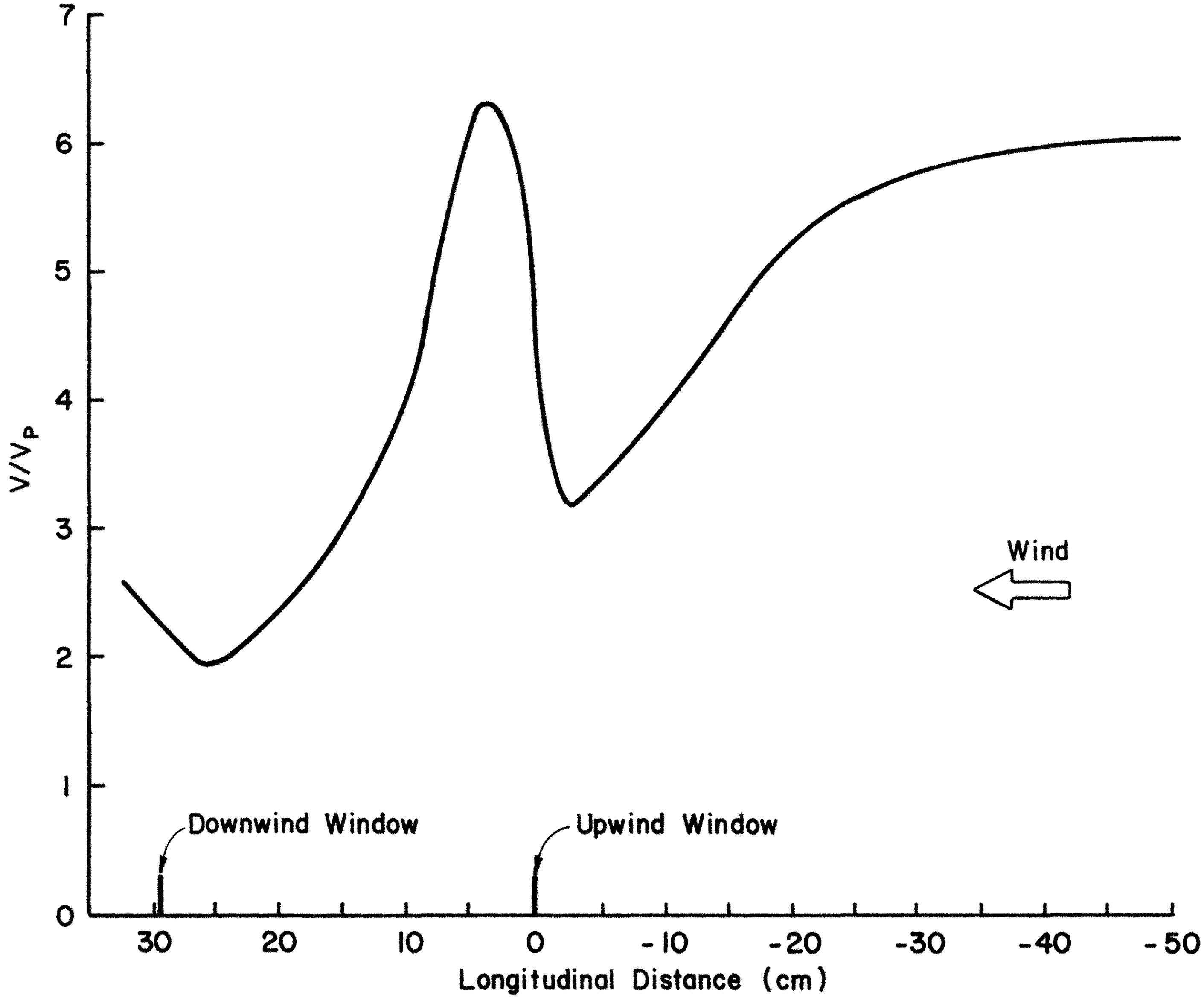


Figure 23. Variation of Velocity Along the Longitudinal Axis of Model Configuration B.

(a)

Inlet A

| | | |
|---|---|---|
| 1.24 | 1.26 | 1.26 |
| 1.06 | 1.04 | 1.10 |
| .85 | .73 | .91 |

Average: 1.05

Outlet A

| | | |
|---|---|---|
| 2.00 | 1.98 | 2.00 |
| 1.95 | 1.81 | 1.95 |
| 2.01 | 1.97 | 2.04 |

Average: 1.97

(b)

Inlet B

| | | |
|---|---|---|
| 1.08 | 1.01 | 1.06 |
| .99 | .94 | 1.00 |
| 1.02 | .92 | 1.01 |

Average: 1.00

Outlet B

| | | |
|---|---|---|
| .49 | .48 | .52 |
| .51 | .51 | .55 |
| .47 | .53 | .51 |

Average: .51

(c)

Inlet C

| | | |
|---|---|---|
| .99 | 1.05 | 1.10 |
| .89 | .93 | .99 |
| .83 | .73 | .85 |

Average: .93

Outlet C

| | | |
|---|---|---|
| .96 | 1.11 | 1.28 |
| .80 | .87 | 1.13 |
| .94 | 1.08 | 1.23 |

Average: 1.04

Figure 24. Schematic Display of Velocity Ratios $[(V/V_p)/(\Delta C_p/C_F)^{\frac{1}{2}}]$ at Model Inlets and Outlets.

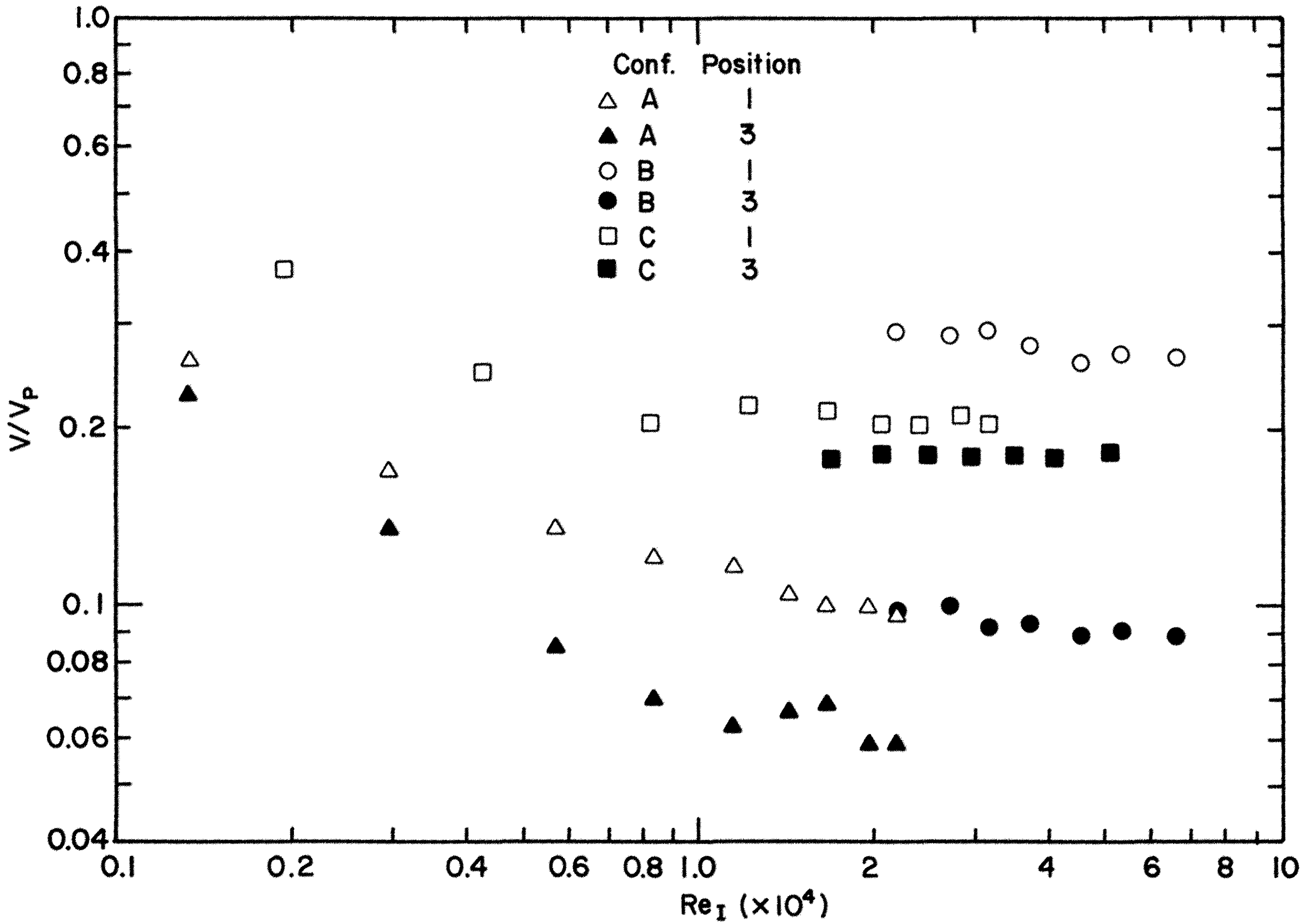


Figure 25. Measured Dimensionless Velocities Inside the Room Plotted Versus the Internal Reynolds Number.

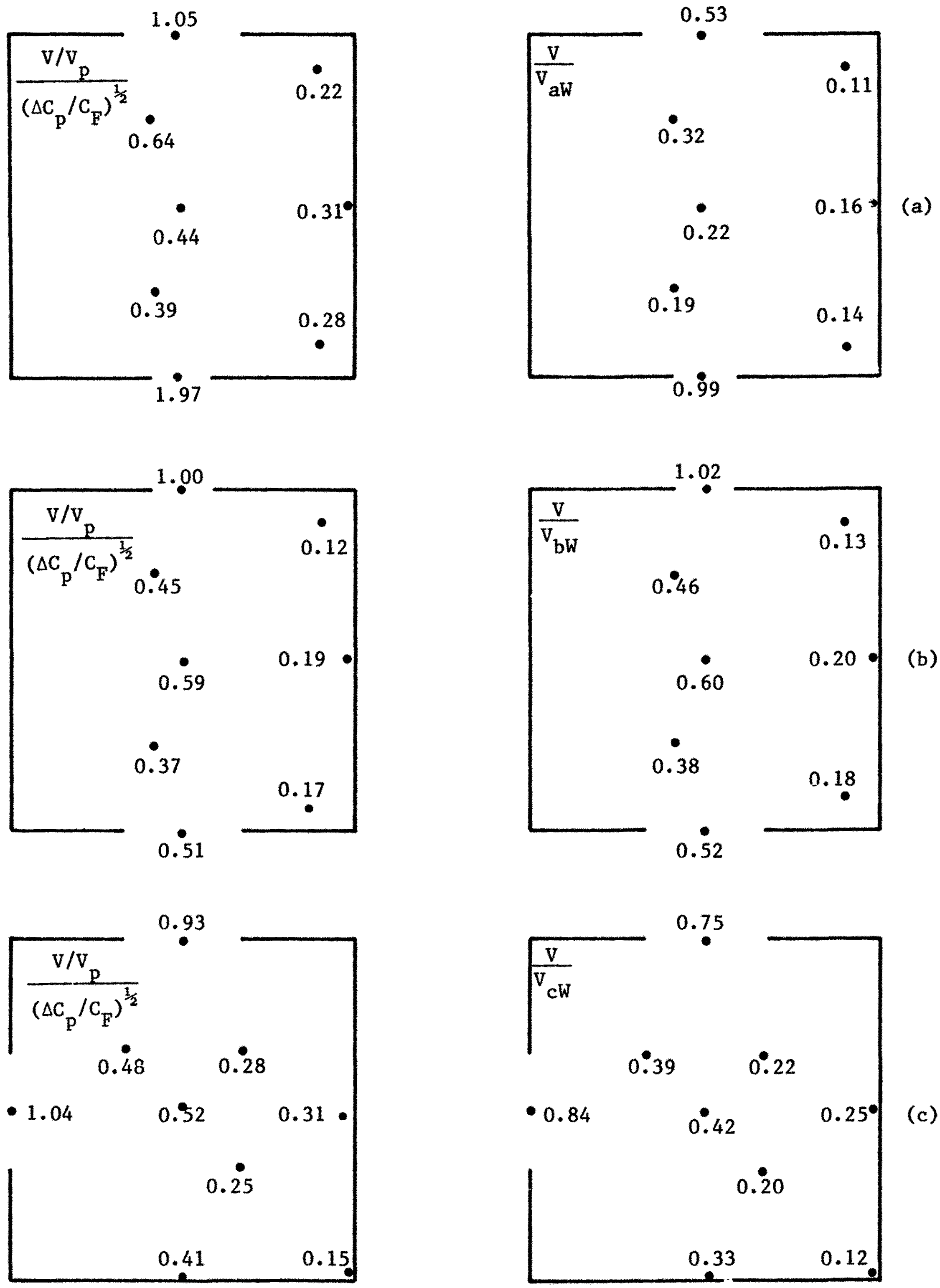


Figure 26. Schematic Display of Velocity Ratios Inside Models.